Brain, Behavior, & Immunity - Health 15 (2021) 100283

Contents lists available at ScienceDirect

Brain, Behavior, & Immunity - Health

journal homepage: www.editorialmanager.com/bbih/default.aspx

T lymphocyte and monocyte subsets are dysregulated in type 1 diabetes patients with peripheral neuropathic pain

Jayden A. O'Brien [a], Helen M. McGuire [b,c], Diana Shinko [c,d], Barbara Fazekas de St Groth [b,c], Marc A. Russo [e], Dominic Bailey [e,f], Danielle M. Santarelli [e], Katie Wynne [g,h], Paul J. Austin [a,*]

[a] School of Medical Sciences, Faculty of Medicine and Health, The University of Sydney, Brain and Mind Centre, 94 Mallett St, Camperdown, NSW, 2050, Australia
[b] Discipline of Pathology, Faculty of Medicine and Health, The University of Sydney, NSW, Australia
[c] Ramaciotti Facility for Human Systems Biology, Charles Perkins Centre, The University of Sydney, NSW, Australia
[d] Sydney Cytometry, The University of Sydney, NSW, Australia
[e] Genesis Research Services, Broadmeadow, NSW, Australia
[f] Hunter Medical Research Institute, New Lambton Heights, NSW, Australia
[g] Department of Diabetes and Endocrinology, John Hunter Hospital, Newcastle, NSW, Australia
[h] School of Medicine and Public Health, University of Newcastle, NSW, Australia

ARTICLE INFO

Keywords:
CD27
Chronic pain
Diabetic neuropathy
FlowSOM
Immunophenotyping
MAPKAPK2
MK2
Mass cytometry
SPADE
Type 1 diabetes

ABSTRACT

Diabetic neuropathic pain is a common and devastating complication of type 1 diabetes, but the mechanism by which it develops and persists is yet to be fully elucidated. This study utilised high-dimensional suspension mass cytometry in a pilot cohort to investigate differences in peripheral blood immunophenotypes between type 1 diabetes patients with (n = 9) and without (n = 9) peripheral neuropathic pain. The abundance and activation of several leukocyte subsets were investigated with unsupervised clustering approaches FlowSOM and SPADE, as well as by manual gating. Major findings included a proportional increase in $CD4^+$ central memory T cells and an absolute increase in classical monocytes, non-classical monocytes, and mature natural killer cells in type 1 diabetes patients with pain compared to those without pain. The expression of CD27, CD127, and CD39 was upregulated on select T cell populations, and the phosphorylated form of pro-inflammatory transcription factor MK2 was upregulated across most populations. These results provide evidence that distinct immunological signatures are associated with painful neuropathy in type 1 diabetes patients. Further research may link these changes to mechanisms by which pain in type 1 diabetes is initiated and maintained, paving the way for much needed targeted treatments.

1. Introduction

Diabetic neuropathic pain (DNP) is a debilitating microvascular complication of diabetes mellitus and affects approximately half of all diabetes patients (Young et al., 1993). Though the presentation of DNP varies widely, it most commonly presents as a symmetrical distal polyneuropathy that preferentially, but not exclusively, affects the lower limbs with burning, tingling, cold, or electrical pain which often worsens at night (Fowler, 2008; Tesfaye et al., 2013). The majority of existing treatments, including anti-neuropathic drugs such as pregabalin, gabapentin, and amitriptyline, aim for relief of pain and related symptoms (Javed et al., 2015; Iqbal et al., 2018), but unfortunately do not consistently offer a 50% reduction in pain (Finnerup et al., 2015) or improve quality of life (Waldfogel et al., 2017; Amato Nesbit et al., 2019).

Type 1 diabetes mellitus (T1D) is characterised by decreased endogenous insulin production by virtue of the autoimmune destruction of insulin-producing pancreatic β-cells (Greenbaum et al., 2017). Evidence from flow and mass cytometry of peripheral blood of T1D patients, as well as mouse models, suggests the association of several leukocyte populations with the disease, including T_h1 cells and $CD8^+$ T cells, regulatory T cells (T_{regs}), natural killer (NK) and natural killer T (NKT) cells, monocytes, macrophages, and dendritic cells (DCs; Rodacki et al., 2007; Lehuen et al., 2010; Sia and Hanninen, 2010; Wong and Wen, 2012; Nel and Lehuen, 2016; Marca et al., 2018; Barcenilla et al., 2019; Wiedeman et al., 2020). Though some of these changes have been associated with the autoimmune component of the condition, the prolonged hyperglycaemia precipitated by this autoimmunity can, in turn, lead to secondary inflammatory changes associated with diabetic complications

* Corresponding author.
E-mail address: paul.austin@sydney.edu.au (P.J. Austin).

https://doi.org/10.1016/j.bbih.2021.100283
Received 5 April 2021; Received in revised form 31 May 2021; Accepted 4 June 2021
Available online 9 June 2021

such as DNP (Zhou and Zhou, 2014). These secondary changes are thought to occur via the increased production of advanced glycation end products (AGEs), which can interact with their receptor (RAGE) to invoke a nuclear factor kappa-B (NFκB)-mediated proinflammatory response (Bierhaus et al., 2005). Peripheral immune changes may then initiate local inflammatory processes that propagate neuropathy and associated pain (Sandireddy et al., 2014; Zhou and Zhou, 2014). However, the precise immunological changes that initiate and propagate DNP, as distinct from those associated with T1D or hyperglycaemia more generally, remain to be fully elucidated.

Neuropathic pain and other chronic pain conditions also display distinct immune signatures which involve shifts in the frequency and activation of macrophages, DCs, and T cells including T_{regs} in the periphery (Austin and Moalem-Taylor, 2010; Luchting et al., 2015; Russo et al., 2019). Pro-inflammatory cytokines, such as tumour necrosis factor (TNF-α), interleukin-1β (IL-1β), and IL-6, are released by infiltrating T cells and macrophages, as well as resident microglia, in peripheral nervous tissue (Moalem et al., 2004; Austin and Moalem-Taylor, 2010; Alvarado-Vazquez et al., 2019; Arman et al., 2020). These cytokines can directly activate c-fibres and result in allodynia and hyperalgesia (Sommer and Kress, 2004). Strong preclinical and clinical evidence suggests that similar temporal and spatial patterns of cytokine signalling may also exist in diabetic neuropathy (Janahi et al., 2015), including infiltration of peripheral macrophages (Sun et al., 2019), microglial activation (Zychowska et al., 2013; Yang et al., 2017), and release of key proinflammatory cytokines including TNF-α, IL-6, C-reactive protein, and TGFβ (Yamakawa et al., 2011; Hussain et al., 2013, 2016; Zhu et al., 2015; Ge et al., 2016). However, evidence that compares peripheral inflammatory states between T1D patients with and without pain remains limited.

This study aimed to investigate the circulating inflammatory correlates of DNP, as distinct from the general T1D immunophenotype, using high-dimensional mass cytometry. This approach allows for a range of major peripheral blood leukocyte populations and their functional states to be detected and compared simultaneously. We expected to find that the subset of immune cells implicated in both T1D and other chronic pain conditions, such as memory T cells (Moalem et al., 2004; Russo et al., 2019) and monocyte populations (Min et al., 2012), would be expanded and activated in participants with DNP compared to T1D patients without DNP.

2. Material and methods

2.1. Ethical approval and participation consent

Experiments received ethical approval from the University of Sydney Human Research Ethics Committee (HREC #2017/019). Authorisation for access to participants who fit the inclusion criteria was granted by the Hunter New England Local Health District. Participation in the study was entirely voluntary, and informed written consent was received from each participant prior to their involvement in the study. Demographic and medical data was deidentified from the researchers and was collected, stored, and retrieved in accordance with state and federal legislation and the University of Sydney's research data management policy.

2.2. Participants

Recruitment of participants was conducted by Genesis Research Services (Broadmeadow, NSW, Australia) from April 2018 to January 2020 in the Newcastle and Greater Hunter Region of New South Wales, Australia. Potential participants were not considered for inclusion if they were aged less than 18 years, were pregnant, presented with non-neuropathic, acute, or mixed pain, had neuropathic pain for less than 3 months, or if any coexisting pain or psychological condition that may confound findings was present. A total of 18 participants with a clinical diagnosis of type 1 diabetes mellitus were included in the study. Of these, half had a clinical diagnosis of painful diabetic peripheral neuropathy (DNP; n = 9). The diagnosis was confirmed with a score of four or greater on the douleur neuropathique 4 questionnaire (DN4; Bouhassira et al., 2005), which measures the presence of tingling, burning, and electric pain via self-report and hypoesthesia via clinical examination. The remaining participants were assigned to the type 1 diabetes-only control group (T1DO; n = 9). T1DO participants were excluded if they had any evidence of painful or painless neuropathy, or any other diabetes-related microvascular complications. The final list of participants consisted of female and male Caucasian Australians 43–71 years of age. Prior to blood collection, all participants participated in a seven-day washout of immunomodulatory medications, including steroids, opioids, and non-steroidal anti-inflammatory drugs. All participants continued taking medication necessary for management of their diabetes.

2.3. Demographic information and questionnaires

Participants provided demographic information, including biological sex, age, ethnicity, and work status. Height and weight were measured from which body mass index (BMI) was calculated. Participants also answered a series of questionnaires which were selected to quantify their self-reported pain-related experiences beyond the presence/absence criteria of diagnosis. These included a visual analogue scale (VAS, 0–100) of pain intensity, the Short-Form McGill Pain Questionnaire (SF-MPQ-2; Dworkin et al., 2009), the Pain Catastrophising Scale (PCS; Sullivan et al., 1995), the Tampa Scale for Kinesiophobia (TSK; Roelofs et al., 2011), the Pain Self-Efficacy Questionnaire (PSEQ; Nicholas, 2007), and the short-form Depression, Anxiety, and Stress Survey (DASS21; Antony et al., 1998). Each of these questionnaires has been previously verified in patient cohorts and provides information on distinct components of the sensory-discriminative, psychological, and behavioural aspects of pain.

2.4. Blood sample collection

Non-fasted whole blood was collected by a trained phlebotomist via venepuncture through the antecubital fossa. Aliquots of whole blood were stored in Smart Tube Proteomic Stabiliser (Smart Tube Inc.; 0.5 mL whole blood/0.7 mL stabiliser per vial) at −80 °C until cell staining.

2.5. Cell staining and time-of-flight acquisition

Whole blood samples were stained with minor modification to the method reported by Russo et al. (2019). A total of 39 markers were chosen, based on previous clinical and preclinical literature, to allow for the identification of key T cell, monocyte, NK cell, and DC populations as well as the quantification of key intracellular transcription factors, enzymes, and other functional markers. All antibodies were validated, pre-titered, and supplied in per-test amounts by the Ramaciotti Facility for Human Systems Biology Mass Cytometry Reagent Bank. Reagent bank antibodies were purchased in a carrier-protein-free form and conjugated by the Ramaciotti Facility for Human Systems Biology with the indicated metal isotope using the MaxPAR® conjugation kit (Fluidigm, South San Francisco, CA) according to the manufacturer's protocol. The panel of antibodies is available in Table 1.

One vial of blood sample per participant (DNP: n = 9; T1DO: n = 9) was thawed and underwent erythrocyte lysis using the Smart Tube Thaw-Lyse Kit (Smart Tube Inc.) per the manufacturer's protocol. Pellets were resuspended in 1 mL fluorescence-activated cell-sorting (FACS) buffer (0.5% BSA, 2 mM EDTA and 0.02% sodium azide in PBS). 10 μL of sample was stained with Trypan blue for haemocytometric cell counts, and 2×10^6 cells were transferred to FACS buffer and centrifuged at 500*g* for 5 min at 4 °C.

Samples were then prepared for palladium-based CD45 barcoding to reduce the effect of any tube-related variation in antibody-dependent signals (Zunder et al., 2015). Cells were blocked with 200 μL heparin (100 IU/mL) in FACS buffer at room temperature for 20 min to reduce

Table 1
Details of the antibody panel used for peripheral blood staining. The conjugated metal, target antigen, clone, supplier, and final concentration of each antibody is reported. The inclusion or exclusion of each antigen in manual gating and FlowSOM analysis is indicated. For manual gating, a tick indicates use of the marker in the manual gating strategy to classify cell populations. For FlowSOM analysis, 'type' markers were included in clustering parameters, while 'state' markers did not contribute to the clustering algorithm but were compared for median expression within clusters. Two markers were conjugated to a fluorophore rather than a metal (pPLCγ2-PE and RORγt-Alexa Fluor 647) and a metal-conjugated anti-secondary antibody (^{175}Lu-anti-PE and ^{147}Sm-anti-Cy5 respectively) was instead used to visualise these markers. Seven markers were excluded from analysis due to suboptimal staining quality. Transcription factors were stained for their phosphorylated form (denoted with a 'p' suffix).

Staining Parameters					Manual Gating	FlowSOM	
Metal	Antigen	Clone	Supplier	Conc. (μg/mL)		$CD3^+$	$CD19^-CD3^-$
^{104}Pd	CD45	HI30	Biolegend	4	✓		
^{106}Pd	CD45	HI30	BD	6	✓		
^{115}In	CD8	RPA-T8	Biolegend	4	✓	Type	
^{141}Pr	CD235ab	HIR2	Biolegend	1.6	✓		
^{142}Nd	CD19	HIB19	Biolegend	1	✓		
^{143}Nd	CD56	REA196	Miltenyi Biotec	0.5	✓	Type	Type
^{144}Nd	TCRγδ	B1	Biolegend	2	✓	Type	
^{145}Nd	CD4	RPA-T4	Biolegend	1	✓	Type	
^{146}Nd	CD123	6H6	Biolegend	0.5	✓		Type
^{147}Sm	Anti-Cy5	CY5-15	Sigma	4	-	–	–
^{148}Nd	CD16	B73.1	BD	1	✓		Type
^{149}Sm	CD25	M-A251	Biolegend	4	✓	Type	
^{150}Nd	pSTAT5	47	BD	6	Excluded		
^{151}Eu	CD39	A1	Biolegend	4		Type	
^{152}Gd	CD66b	G10F5	BD	3 μL/mL	✓		
^{153}Eu	pSTAT1	14/P-STAT1	BD	2	Excluded		
^{154}Gd	pAKT	J1.233.371	BD	4		State	State
^{155}Gd	CD27	M-T271	BD	1		State	
^{156}Gd	pp38 MAPK	30/p38 MAPK	BD	4	Excluded		
^{158}Gd	pSTAT3	4/P-STAT3	BD	8	Excluded		
^{159}Tb	CD197 (CCR7)	150503	R&D Systems	6	Excluded		
^{160}Gd	CD14	M5E2	BD	4	✓		Type
^{161}Dy	CD141	AD5-14H12	Miltenyi Biotec	8	✓		Type
^{162}Er	Foxp3	PCH101	eBioscience	3		Type	
^{163}Dy	CD1c (BDCA-1)	L161	Biolegend	1	✓		Type
^{164}Er	CD45RO	UCHL1	BD	6		Type	
^{165}Ho	CD61	VI-PL2	Biolegend	2	✓		
^{166}Er	pp65 NFκB	K10–895.12.50	BD	4		State	State
^{167}Er	CD11c	Bu15	Biolegend	2	✓		Type
^{168}Er	pERK1/2	4B11B69	Biolegend	2		State	State
^{169}Tm	CD45RA	HI100	BD	2	✓	Type	
^{170}Er	CD3	UCHT1	Biolegend	2	✓	State	
^{171}Yb	CD62L	DREG-56	Biolegend	4	✓	Type	
^{172}Yb	CD130 (gp130)	AM64	BD	8		State	State
^{173}Yb	pMK2	P24-694	BD	4		State	State
^{174}Yb	HLA-DR	L243	Biolegend	2	✓		Type
^{175}Lu	Anti-PE	PE001	Biolegend	4	-	–	–
^{176}Lu	CD127 (IL-7Rα)	A019D5	Biolegend	2	✓	Type	State
^{209}Bi	T-bet	4B10	BD	2	Excluded		
PE	pPLCγ2	K86–689.37	BD	200 μL/mL		State	State
AF647	RORγt	Q21-559	BD	4	Excluded		

eosinophil-related artefacts (Rahman et al., 2016). DNP samples were incubated with ^{106}Pd-CD45 while T1DO samples were incubated with ^{104}Pd-CD45 in 50 μL volume for 30 min on ice, followed by washing. Pairs containing one DNP and one T1DO sample were then combined for further processing in the same tube. Paired samples were age- and sex-matched, where possible. Cells were blocked with heparin as before, stained with surface antibodies in 100 μL FACS buffer for 30 min on ice, washed three times in FACS buffer, and resuspended in 0.5 mL transcription factor fixation/permeabilisation buffer (eBioscience™; 1:3 concentrate to diluent) and incubated at 4 °C overnight.

The next day, intracellular antibody staining was performed. Cells were washed twice in 1 mL permeabilisation buffer (eBioscience), heparin blocked, and incubated for 30 min with 100 μL intracellular antibody cocktail in permeabilisation buffer on ice. After washing in FACS buffer, cells were resuspended in residual volume, and 500 μL of 100% cold methanol was added dropwise and then incubated on ice for 30 min. After a FACS wash and a heparin block in FACS buffer as before, samples were incubated with 100 μL nuclear antibodies in FACS buffer for 30 min on ice, followed by fluorescent secondary antibodies (anti-PE and anti-AF647) in 100 μL FACS buffer for 20 min on ice to allow detection of primary antibodies without a directly conjugated metal. Cells were then incubated with 200 μL of 1:4000 Cell ID DNA intercalator (Fluidigm) in 4% paraformaldehyde for 20 min at room temperature and then kept at 4 °C until acquisition.

Immediately before acquisition, cells were washed twice in ultrapure water and once in cell acquisition solution (CAS; Fluidigm). Cells were counted and then resuspended at 8×10^5 cells/mL in 1:10 EQ™ Four Element Calibration Bead solution (Fluidigm) in CAS. The suspension was filtered using a 5 mL round bottom polystyrene test tube with cell strainer snap cap to remove debris and aggregates. Data from blood samples were acquired with a time-of-flight mass cytometer (Helios™, a CyTOF® system, Fluidigm). Output.fcs files were bead-normalised (Finck et al., 2013) using CyTOF software (Fluidigm).

2.6. Unsupervised clustering analysis

2.6.1. SPADE

Spanning-tree progression analysis of density-normalised events (SPADE) was conducted using freely available SPADE V3.0 standalone software (Qiu et al., 2011; Qiu, 2017). Cell numbers were

deterministically downsampled from all samples to provide a pooled maximum of 50 000 cells included for analysis which were clustered with a *k*-means of 100. Expression values were arcsinh-transformed with a cofactor of 5. The resulting SPADE tree was visually inspected for major leukocyte populations using phenotypic markers, and similar clusters were annotated according to their shared identity. Each cluster was overlayed with a colour scale signifying the ratio of median expression between DNP and T1DO samples of a functional marker in that cluster of cells. No statistical analyses were conducted on these results; the visualisations were used to recognise trends in expression patterns across populations which were later interrogated quantitatively using FlowSOM and manual gating.

2.6.2. FlowSOM

Classification of cell subsets was conducted using FlowSOM, an unsupervised clustering and visualisation technique (Van Gassen et al., 2015). The artificial neural network approach utilises self-organising maps to hierarchically group multidimensional cytometry data into clusters of phenotypically similar cells, which can be analysed for the differential abundance and expression of structural and functional markers included in the antibody panel.

FlowSOM was conducted in R using the CATALYST package (Crowell et al., 2020) on .fcs files manually pre-gated as either $CD3^+$ (T cells) or $CD19^-CD3^-$ (NK cells, monocytes, and DCs). $CD19^+$ B cells were included as a third subset in preliminary analysis, but the resulting FlowSOM clusters proved uninformative, likely due to the paucity of B cell-specific markers included in the antibody panel. The workflow used for this study was in part adapted from Nowicka et al. (2017). $CD3^+$ pre-gated cells were sorted into a 12 × 12 map, giving 144 total clusters, which then underwent unsupervised metaclustering into 30 metaclusters using the ConsensusClusterPlus algorithm. $CD19^-CD3^-$ pre-gated cells used a 10 × 10 clustering matrix, giving 100 total clusters, which were sorted into 20 metaclusters. These parameters provided sufficient metaclusters to capture the expected number of unique cell types while potentially uncovering other biologically interesting populations. The panel of markers used in the clustering algorithm for each pre-gated population are available in Table 1.

The resulting metaclusters were manually inspected for marker expression using the heatmap, boxplot, and expression density visualisation tools available within CATALYST (see appendix). Metaclusters were manually merged if the difference between them was negligible; they were excluded entirely if their expression pattern suggested the inclusion of multiple distinct cell populations or non-cell events. Final merged metacluster groupings ($CD3^+$: n = 19, $CD19^-CD3^-$: n = 12) were then manually classified into biologically relevant cell types. Metacluster frequency and functional state marker expression data were exported to GraphPad Prism 9 for differential analysis.

2.7. Manual gating

Verification of FlowSOM clustering, and classification of small cell populations which FlowSOM could not resolve, was conducted using a manual gating strategy adapted from Russo et al. (2019; Fig. 1). The peripheral blood mononuclear cell (PBMC) fraction of acquired events was isolated using FlowJo 10.6 (BD, OR, USA) before further analysis. Normalisation beads were excluded, then cell singlets were selected based on the DNA^+ gate. Paired pain and control samples within a tube were gated for the expression of ^{106}Pd-CD45 and ^{104}Pd-CD45 respectively, with double-positive and double-negative events excluded. The two resulting populations within a tube were exported as individual .fcs files, after which granulocytes ($CD61^+$, $CD66b^+$) and erythrocytes ($CD235ab^+$) were gated out of each sample.

The remaining acquired events were manually gated into cell phenotypes of interest in FlowJo (see Fig. 1). CD62L was used to gate for effector and non-effector T cell subsets since gating by CCR7 expression gave imperfect differentiation of cell populations, as previously observed in this laboratory after exposure of cells to Smart Tube Buffer (Russo et al., 2019). Gated populations were then compared for cell frequency and median expression of functional markers between experimental groups.

2.8. Statistical analysis

The proportion of male and female participants between groups was compared using Fisher's exact test. Other demographic and questionnaire data were compared with unpaired *t*-tests for Gaussian data, and the Mann-Whitney *U* test for non-Gaussian data as determined by the Shapiro-Wilk test. Cell frequencies for manually gated and FlowSOM-generated cell populations were expressed either as a proportion of a parent or grandparent gate, or by absolute cell numbers normalised per mL of whole blood based on haemocytometric counts performed after erythrocyte lysis. Outliers were removed using the ROUT method with Q = 1%. Unpaired *t*-tests or Mann-Whitney *U* tests were used to compare cell frequencies between DNP and T1DO samples. Results are expressed as group means ± standard error of the mean (SEM) unless otherwise indicated.

Median expression values were first arcsinh-transformed with a cofactor of 5, the standard transformation used for mass cytometry data (Olsen et al., 2019). Expression values were then compared using two-way ANOVA with correction for multiple comparisons performed by controlling the false-discovery rate (FDR), using the Benjamini-Hochberg procedure with $q < 0.1$. This method has been used in similar studies (Russo et al., 2019) and is suitable for exploratory immunophenotyping studies with many related comparisons since the increased likelihood of a type 1 error is unlikely to affect the overall interpretation of results. Correlations were conducted using Spearman's rank-order test. Statistical tests and visualisations were produced with GraphPad Prism 9. The significance threshold for all analyses was set at $\alpha = 0.05$.

3. Results

3.1. Demographic and questionnaire data

The proportion of female to male participants was not significantly different between groups ($P = 0.3348$). Though the mean age was somewhat higher in the DNP group, this difference did not reach significance ($t_{16} = 1.913$, $P = 0.0738$). The weight and body mass index (BMI) of DNP participants were significantly higher than that of T1DO participants (weight: $t_{16} = 3.406$, $P = 0.0036$; BMI: $t_{16} = 2.484$, $P = 0.0244$).

The degree of pain reported by DNP participants using a visual analogue scale was significantly higher than the T1DO group ($t_{16} = 7.658$, $P < 0.0001$), with the DNP group reporting a mean of 60/100 on the scale. This was confirmed by a significant increase in the Short-Form McGill Pain Questionnaire (SF-MPQ-2) score in the DNP group (DNP mean = 88/220, $U = 0$, $P < 0.0001$). Additionally, levels of pain catastrophising ($t_{16} = 4.838$, $P = 0.0002$) and kinesiophobia ($t_{16} = 5.184$, $P < 0.0001$) were increased in the DNP group, while ratings of pain self-efficacy were decreased ($U = 5.500$, $P = 0.0009$). The DASS21 revealed increased self-reported depression ($t_{16} = 2.673$, $P = 0.0167$), anxiety ($t_{16} = 3.454$, $P = 0.0033$), and stress ($U = 18$, $P = 0.0467$) in the DNP group. These results are summarised in Table 2.

3.2. SPADE

CD127 expression was strongly increased in $CD4^+$ memory T cells in the DNP group (Fig. 2a), while expression of CD130 (gp130; Fig. 2b) and CD27 (Fig. 2c) was increased in select $CD4^+$ T cell clusters. pp65 NFκB was increased in T cells and decreased in all other populations (Fig. 2d). There were no distinct trends in pAKT expression (Fig. 2e). Other markers were unchanged in T cells between groups but decreased in innate cells, including pERK1/2 (Fig. 2f), and pPLCγ2 (Fig. 2g).

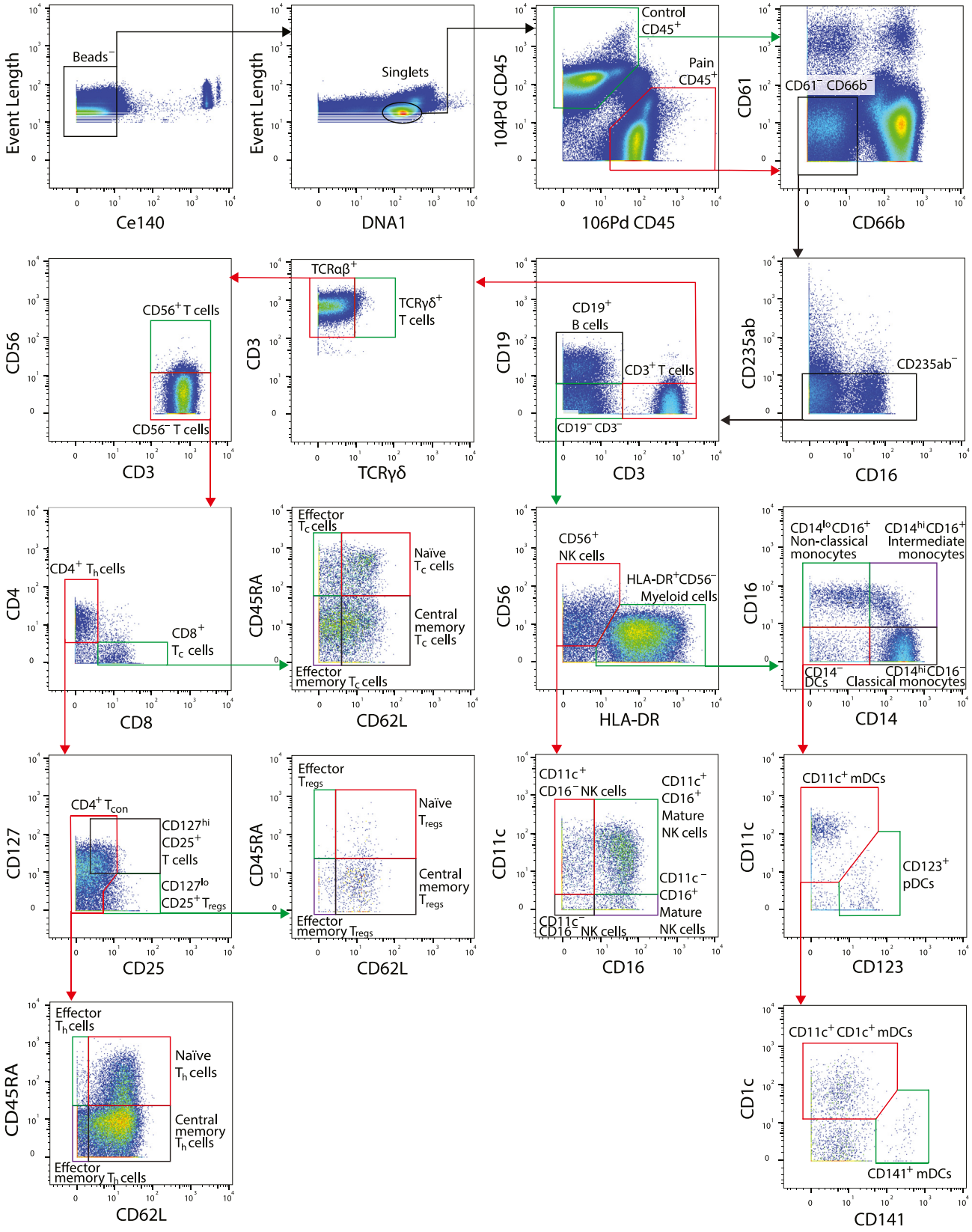

Fig. 1. Manual gating strategy for categorisation of leukocytes from a representative acquisition tube. Pseudocolour biaxial plots represent the density of cells with the indicated expression of the two markers. The coloured boxes and arrows indicate the subpopulation of cells that were selected for application of the following gate. The ^{104}Pd-CD45 and ^{106}Pd-CD45 gates were used to separate DNP and T1DO samples in the same tube. Both populations were then analysed according to the rest of the strategy, though only the DNP sample is shown for subsequent gates here. Gate thresholds were determined by manually inspecting a combination of pseudocolour (shown) and contour plots.

Table 2
Demographic information and questionnaire results for diabetic neuropathic pain patients compared to type 1 diabetes-only controls. Body mass index and weight were significantly increased in the DNP group. DNP patients scored higher for pain, pain catastrophising, kinesiophobia, depression, anxiety, and stress – and scored lower for pain self-efficacy – compared with T1DO controls. BMI: body mass index. DN4: douleur neuropathique 4. VAS: visual analogue scale. SF-MPQ-2: Short-Form McGill Pain Questionnaire 2. PCS: Pain Catastrophising Scale. TSK: Tampa Scale of Kinesiophobia. PSEQ: Pain Self-Efficacy Questionnaire. DASS21: Short-Form Depression, Anxiety and Stress Scale. Data presented as group means ± SEM. T1DO: n = 9; DNP: n = 9. *$P < 0.05$. **$P < 0.01$. ***$P < 0.001$. ****$P < 0.0001$.

		T1DO	DNP
Sex (F/M)		5/4	2/7
Age		55.78 ± 3.8	63.89 ± 1.9
Height (cm)		170.7 ± 2.1	174.3 ± 2.3
Weight (kg)		87.89 ± 5.0	110.7 ± 4.5**
BMI		29.78 ± 1.3	35.37 ± 1.8*
Work status (working/not working)		6/3	2/7
Time since DNP symptom onset (years)			11.11 ± 3.4
Time since DNP diagnosis (years)			8.444 ± 2.7
Affected lower limb (left/right/both)			0/0/9
Affected upper limb (left/right/both)			1/0/1
DN4 score			5.556 ± 0.4
Pain intensity (VAS, 0–100)		3.444 ± 1.3	60.22 ± 7.3****
SF-MPQ-2 (0–220)		1.333 ± 0.6	87.56 ± 15.2****
PCS (0–52)		1.667 ± 0.9	26.44 ± 5.0***
TSK (0–68)		29.89 ± 1.2	44.33 ± 2.5****
PSEQ (60–0)		57.22 ± 1.4	42.67 ± 3.9***
DASS21 (0–42)	Depression	2.222 ± 1.1	12.67 ± 3.8*
	Anxiety	2.000 ± 1.2	13.11 ± 3.0**
	Stress	6.444 ± 3.0	15.11 ± 3.6*

Strikingly, pMK2 expression increased across nearly all cell populations in the DNP group (Fig. 2h).

3.3. Quantitative PBMC analysis

Cell identities were first evaluated by FlowSOM. Manual gating was then used to both confirm the FlowSOM results and to investigate low-abundance cell populations which FlowSOM was unable to resolve, such as naïve, effector, and central memory regulatory T cells.

3.3.1. T cells

FlowSOM metaclustering for $CD3^+$ events revealed 19 cell populations of interest within the $CD3^+$ pre-gate. Most T cell subsets were split into $CD127^{hi}$ and $CD127^{lo}$ subsets, which were combined for abundance analysis but kept separate for analysis of marker expression values. Since there was no difference in the frequency of $CD3^+$ cells between groups ($P = 0.7676$), which suggests that the size of the overall T cell compartment did not increase, subset frequencies were represented as a percentage of total $CD3^+$ cells for each subject to determine whether any phenotypic shifts occurred.

3.3.1.1. Cell frequencies. As a proportion of all $CD3^+$ cells, there was a significant increase in $CD4^+$ T cells in the DNP group (DNP: 75.0 ± 2.89%, T1DO: 60.1 ± 3.92%, $t_{16} = 3.063$, $P = 0.0074$), but no difference in the proportion of $CD8^+$ T cells (DNP: 22.1 ± 2.97%, T1DO: 32.2 ± 4.57%, $t_{16} = 1.848$, $P = 0.0832$; Fig. 3a). Within $CD4^+$ T cells, there was a specific and significant increase in $CD4^+$ central memory T cells in the DNP group compared to T1DO controls (DNP: 24.1 ± 2.38%, T1DO: 12.4 ± 2.83%, $t_{16} = 3.147$, $P = 0.0062$) but no difference in naïve, effector, or effector memory $CD4^+$ T cells (all $P > 0.05$; Fig. 3b). In contrast, $CD8^+$ naïve T cells were significantly decreased in the DNP group (DNP: 3.55 ± 0.489%, T1DO: 12.6 ± 3.50%, $t_{16} = 2.570$, $P = 0.0205$), while all other $CD8^+$ T cell subsets were not significantly different (all $P > 0.05$; Fig. 3c). There were no differences in the abundance of $CD4^+CD39^+$ central memory T cells, $CD39^{hi}$ or $CD39^{lo}$ effector memory T_{regs}, $CD56^+$ T cells, or γδ T cells between groups.

Manual gating confirmed the significant increase in $CD4^+$ T cells (Fig. 3d), though the difference in $CD4^+$ central memory T cells did not reach significance (DNP: 31.8 ± 2.88%, T1DO: 23.5 ± 2.70%, $t_{16} = 2.115$, $P = 0.0504$; Fig. 3e). The decrease in $CD8^+$ naïve T cells was confirmed by manual gating ($P < 0.05$; Fig. 3f). Novel findings uncovered by manual gating (data not shown) included a decrease in effector T_{regs}, as a proportion of all T_{regs}, in the DNP group (DNP: 1.12 ± 0.194%, T1DO: 2.90 ± 0.515%, $t_{16} = 3.229$, $P = 0.0052$) and an increase in $CD127^{hi}CD25^+$ T cells (DNP: 31739 ± 3507 cells/mL, T1DO: 17969 ± 3935 cells/mL, $t_{16} = 2.612$, $P = 0.0189$). Taken together, these results suggest that T cells are polarised toward a $CD4^+$ central memory phenotype in DNP.

3.3.1.2. Functional marker expression. Analysis of expression values within FlowSOM metaclusters revealed an increase in phospho-MK2 (pMK2) expression across most T cell subsets in DNP samples, with many increasing by over two-fold. There were significant increases in pMK2 expression in $CD4^+CD127^{hi}$ ($q = 0.0049$, $P = 0.0014$), $CD4^+CD127^{lo}$ ($q = 0.0094$, $P = 0.0027$), and $CD4^+CD39^+$ ($q = 0.0307$, $P = 0.0088$) central memory T cells; $CD4^+CD127^{hi}$ ($q = 0.0091$, $P = 0.0021$) and $CD4^+CD127^{lo}$ ($q = 0.0631$, $P = 0.0090$) effector memory T cells; $CD4^+CD39^{hi}$ ($q = 0.0554$, $P = 0.0158$) and $CD4^+CD39^{lo}$ ($q = 0.0314$, $P = 0.0090$) effector memory T_{regs}; $CD8^+CD127^{hi}$ ($q = 0.0312$, $P = 0.0089$) and $CD4^+CD127^{lo}$ ($q = 0.0870$, $P = 0.0249$) naïve T cells; $CD8^+$ central memory T cells ($q = 0.0009$, $P = 0.0002$); $CD8^+CD127^{hi}$ ($q = 0.0022$, $P = 0.0004$) and $CD8^+CD127^{lo}$ ($q = 0.0492$, $P = 0.0070$) effector memory T cells; and γδ T cells ($q = 0.0857$, $P = 0.0245$). These differences are summarised in Fig. 4.

CD27 expression was also elevated in DNP patients on several T cell populations, largely corresponding to the populations expressing increased pMK2. These included $CD4^+$ naïve T cells ($q = 0.0847$, $P = 0.0121$); $CD4^+CD127^{hi}$ ($q < 0.0001$, $P < 0.0001$), $CD4^+CD127^{lo}$ ($q = 0.0013$, $P = 0.0002$), and $CD4^+CD39^+$ ($q = 0.0307$, $P = 0.0080$) central memory T cells; $CD4^+CD127^{hi}$ effector memory T cells ($q = 0.0091$, $P = 0.0026$); $CD39^{hi}$ ($q = 0.0009$, $P = 0.0001$) and $CD39^{lo}$ ($q = 0.0061$, $P = 0.0009$) effector memory T_{regs}; $CD8^+CD127^{hi}$ ($q = 0.0153$, $P = 0.0022$) and $CD8^+CD127^{lo}$ ($q = 0.0870$, $P = 0.0213$) naïve T cells; $CD8^+$ central memory T cells ($q = 0.0002$, $P < 0.0001$); and $CD8^+CD127^{hi}$ effector memory T cells ($q = 0.0022$, $P = 0.0006$). CD27 expression was significantly decreased on γδ T cells ($q = 0.0857$, $P = 0.0204$; Fig. 4).

Expression of phospho-p65 NFκB was significantly upregulated in $CD8^+$ central memory T cells ($q = 0.0748$, $P = 0.0320$) and $CD8^+CD127^{hi}$ effector memory T cells ($q = 0.0022$, $P = 0.0006$). No other pp65 NFκB differences were significant, though there was a general trend toward upregulation across the entire $CD3^+$ compartment (Fig. 4). No other markers analysed on T cells were significantly different between groups. Together, these results point toward a role for $CD4^+$ central memory T cells, CD27, pMK2, and pp65 NFκB in DNP beyond that which exists in T1D alone.

Manual gating confirmed the upregulation of pMK2 and CD27 in most T cell populations, with additional increases in $CD56^+$ T cells and naïve and central memory T_{regs} (data not shown). A novel finding was the increase in CD39 expression on central memory ($q = 0.0296$, $P = 0.0068$) and effector memory ($q = 0.0123$, $P = 0.0019$) T_{regs} (Fig. 5a). In addition, CD127 expression was increased on memory $CD4^+$ T cells, including central memory ($q = 0.0010$, $P = 0.0002$) and effector memory ($q = 0.0155$, $P = 0.0013$) $CD4^+$ T cells in the DNP group (Fig. 5b). These results indicate a role for CD39 on memory T_{regs} and CD127 on $CD4^+$ memory T cells in DNP.

3.3.2. NK cells, monocytes, and dendritic cells

A total of 12 metaclusters were defined by FlowSOM analysis in the $CD19^-CD3^-$ pre-gate, including NK cells, monocytes, and DCs. Since the difference in total $CD19^-CD3^-$ cells between groups approached significance ($P = 0.1044$), and proportional data may therefore be misleading,

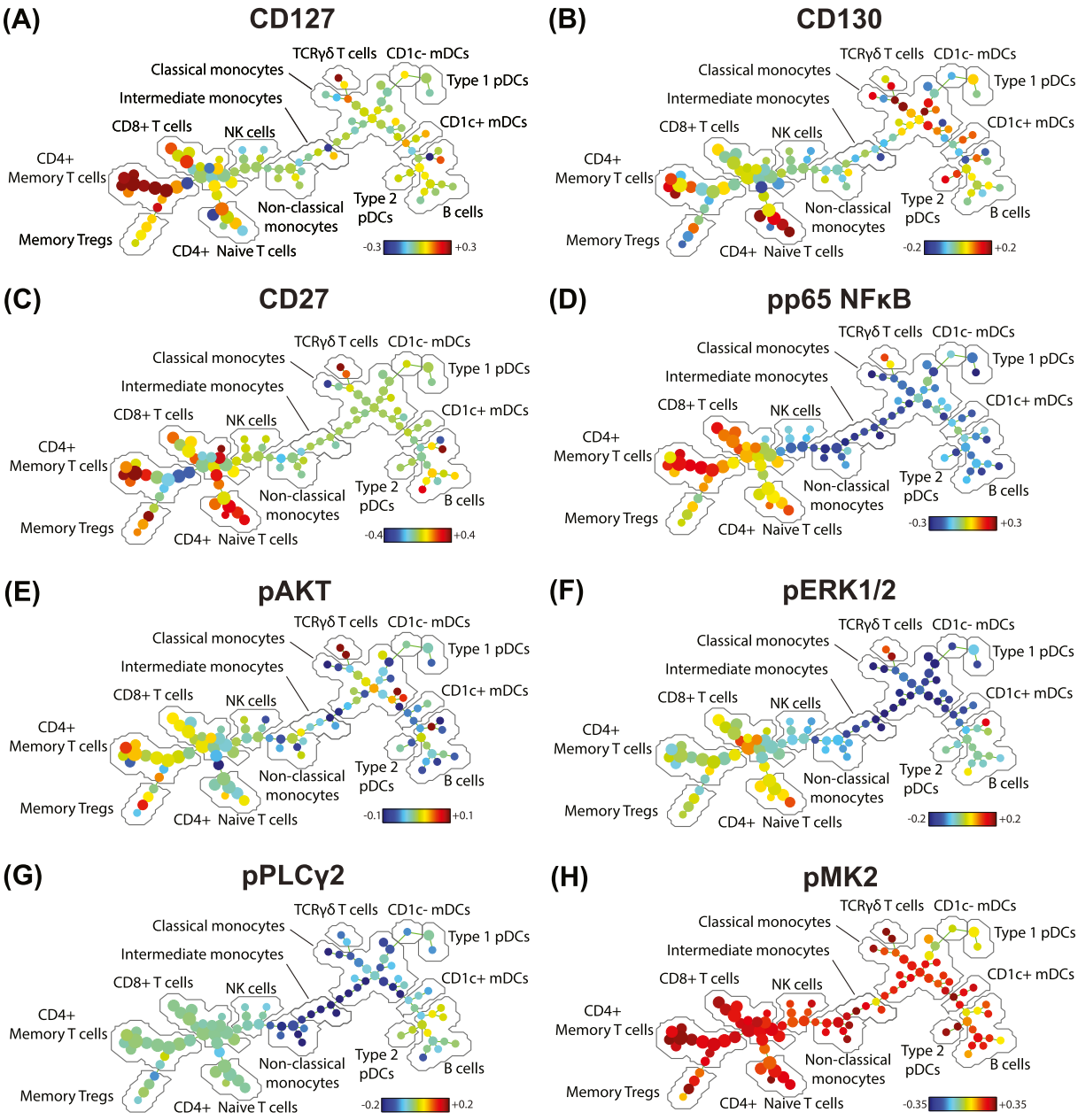

Fig. 2. SPADE trees indicating the relative median expression of selected functional markers across clusters of PBMCs. Each node in the tree represents one cluster of cells grouped based on phenotypic similarities as determined by the SPADE algorithm. The distance between nodes represents their degree of phenotypic similarity. The colour of each node denotes the ratio of arcsinh-transformed expression between DNP patients and T1DO controls; red indicates increased expression in the DNP group compared to controls, and blue indicates decreased expression. The colour scale differs between markers. **(A)** CD127, **(B)** CD130, **(C)** CD27, **(D)** pp65 NFκB, **(E)** pAKT, **(F)** pERK1/2, **(G)** pPLCγ2, **(H)** pMK2. (For interpretation of the references to colour in this figure legend, the reader is referred to the Web version of this article.)

cell frequency results were represented in terms of absolute frequency per mL of whole blood to account for the potential increase in cell number within some cell subpopulations.

3.3.2.1. Cell frequencies. FlowSOM detected no significant differences in NK cell abundance, though there were notable upward trends in total $CD56^+$ NK cells (DNP: 76752 ± 12292 cells/mL, T1DO: 48537 ± 6199 cells/mL, $t_{15} = 1.970$, $P = 0.0676$) and particularly in $CD56^+CD16^+$ mature NK cells (DNP: 69094 ± 11724 cells/mL, T1DO: 44424 ± 6158 cells/mL, $t_{15} = 1.794$, $P = 0.0931$) in the DNP group (Fig. 6a).

There was a significant increase in the frequency of $CD14^+CD16^-$ classical monocytes (DNP: 130242 ± 16043 cells/mL, T1DO: 78436 ± 17231 cells/mL, $t_{16} = 2.200$, $P = 0.0428$) and $CD14^-CD16^+$ non-classical monocytes (DNP: 27986 ± 4332 cells/mL, T1DO: 15603 ± 3280 cells/mL, $t_{16} = 2.279$, $P = 0.0367$), but not $CD14^+CD16^+$ intermediate monocytes (DNP: 4787 ± 1022 cells/mL, T1DO: 3146 ± 1095 cells/mL, $t_{16} = 1.096$, $P = 0.2893$) in the DNP group (Fig. 6b). No mDC or pDC population frequencies were significantly different between groups. Taken together, these results suggest the strong involvement of classical and non-classical monocytes in DNP.

Since increased monocyte frequency – monocytosis – is associated with obesity (Nagareddy et al., 2014), Spearman's correlation was used to determine whether a relationship existed between BMI and classical monocyte frequency. While these variables were positively correlated in the T1DO group ($r = 0.68$, $P = 0.0486$), the relationship did not hold in the DNP group ($r = 0.10$, $P = 0.8100$). This suggests that the increased

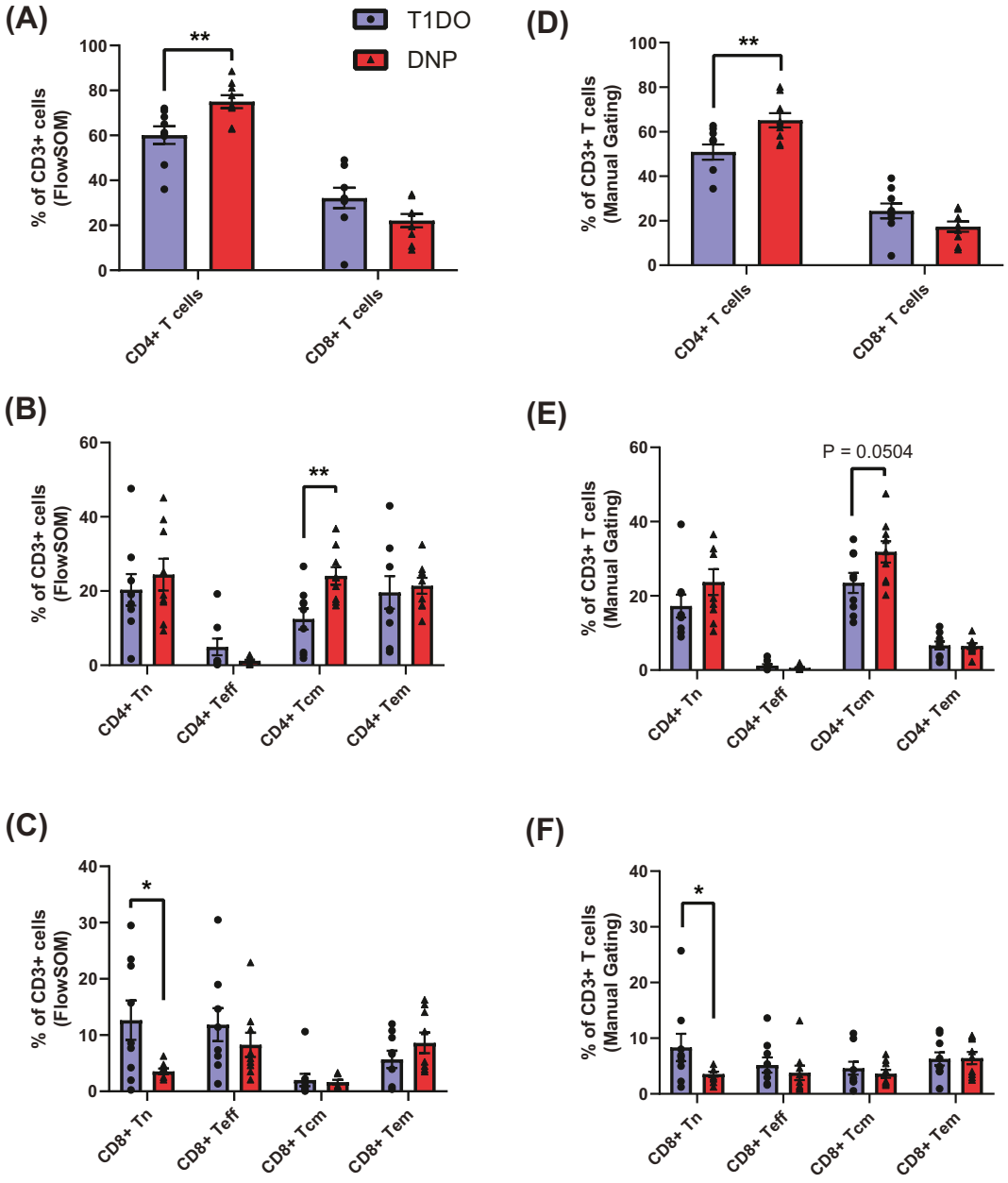

Fig. 3. Frequency of T cell subpopulations as defined by FlowSOM metaclusters **(A–C)** and manual gates **(D–F)**. **(A)** The $CD4^+$ T cell compartment was significantly expanded in the DNP group, while the corresponding decrease in proportion of $CD8^+$ cells did not reach statistical significance. **(B)** The proportion of $CD4^+$ T cells with a central memory ($CD45RO^+CD62L^+$) phenotype was doubled in the DNP group compared to T1DO controls. **(C)** $CD8^+$ naïve T cells significantly decreased their proportion in the DNP group. **(D)** Manual gating confirmed the $CD4^+$ T cell increase, **(E)** demonstrated a trend toward an increase in $CD4^+$ central memory T cells which did not reach significance, and **(F)** confirmed the decrease in $CD8^+$ naïve T cells. Columns represent group means ± SEM where each data point represents an individual patient. T_n: naïve T cells; T_{eff}: effector T cells; T_{cm}: central memory T cells; T_{em}: effector memory T cells. Unpaired *t*-test or Mann-Whitney *U* test: $*P < 0.05$; $**P < 0.01$.

BMI in the DNP group did not adequately explain the expansion of the monocyte compartment in these patients (Fig. 6c).

When investigated by manual gating, the upward trend in NK cell frequency uncovered by FlowSOM reached significance. There was a significant increase in total $CD56^+$ NK cells (DNP: 94366 ± 11089 cells/mL, T1DO: 56168 ± 7312 cells/mL, $t_{14} = 2.876$, $P = 0.0122$), which was explained by a selective significant increase in $CD16^+$ mature NK cells (DNP: 75957 ± 10502 cells/mL, T1DO: 43157 ± 5644 cells/mL, $t_{14} = 2.751$, $P = 0.0156$; Fig. 6d). Absolute increases in classical and non-classical monocytes were confirmed ($P < 0.05$; Fig. 6e). When NK cells were split into $CD11c^+$ and $CD11c^-$ subsets by manual gating, there was a specific increase in $CD11c^+$ mature NK cells (DNP: 55419 ± 9056 cells/mL, T1DO: 29992 ± 4947 cells/mL, $t_{14} = 2.464$, $P = 0.0273$; Fig. 6f). These results point toward the involvement of mature NK cells, classical monocytes, and non-classical monocytes in DNP.

3.3.2.2. Functional marker expression. FlowSOM revealed that pMK2 was upregulated on most $CD19^-CD3^-$ metaclusters, including $CD16^-CD11c^+$ NK cells ($q = 0.0619$, $P = 0.0088$); $CD16^+CD11c^+$ ($q = 0.0938$, $P = 0.0134$) and $CD16^+CD11c^-$ ($q = 0.0940$, $P = 0.0134$) mature NK cells; classical ($q = 0.0966$, $P = 0.0138$), intermediate ($q = 0.0886$, $P = 0.0127$), and non-classical ($q = 0.0092$, $P = 0.0013$) monocytes; $CD11c^+CD1c^+$ mDCs ($q = 0.0403$, $P = 0.0058$); and $CD123^+$ pDCs ($q = 0.0092$, $P = 0.0013$). When combined with the $CD3^+$ results, this

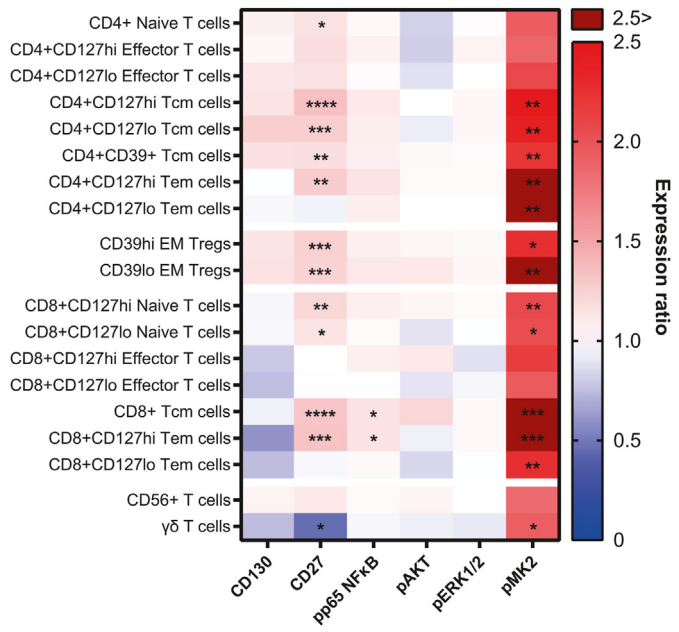

Fig. 4. Heatmap displaying the ratio of group means of arcsinh-transformed median expression values for functional state markers in $CD3^+$ FlowSOM metaclusters. A ratio of one (white) indicates that the DNP and T1DO group means are the same. A ratio greater than one (red) indicates DNP > T1DO, while a ratio less than one (blue) indicates DNP < T1DO. Crimson squares indicate a ratio >2.5. Asterisks denote the statistical significance of the difference between group means for a functional state marker in a cell population based on two-way ANOVAs with $q < 0.1$. T_{cm}: central memory T cells; T_{em}: effector memory T cells; EM T_{reg}: effector memory regulatory T cell. Two-way ANOVA with FDR $q < 0.1$: $^*P < 0.05$; $^{**}P < 0.01$; $^{***}P < 0.001$; $^{****}P < 0.0001$. (For interpretation of the references to colour in this figure legend, the reader is referred to the Web version of this article.)

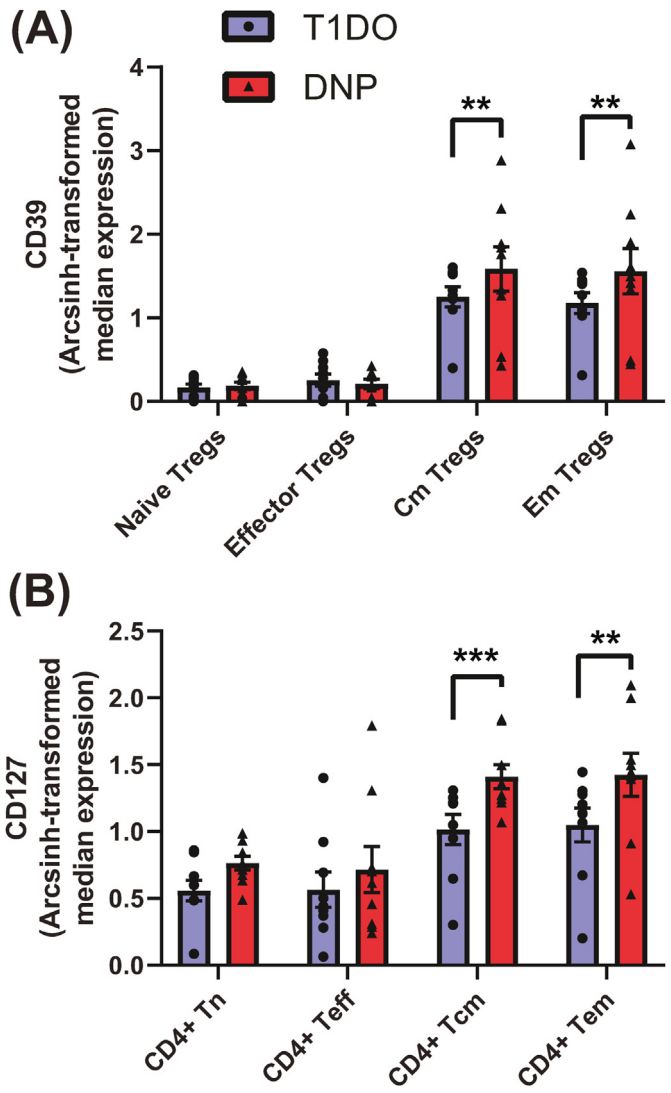

Fig. 5. Novel median expression findings in the $CD3^+$ compartment for functional markers investigated by manual gating only. **(A)** CD39 expression significantly increased on central memory and effector memory T_{regs} in DNP patients, while **(B)** CD127 expression significantly increased in $CD4^+$ central and effector memory T cells. Values represent group means ± SEM. T_{reg}: regulatory T cell; T_n: naïve T cell; T_{eff}: effector T cell; cm: central memory; em: effector memory. Two-way ANOVA with FDR $q < 0.1$: $^{**}P < 0.01$; $^{***}P < 0.001$.

suggests a global upregulation of pMK2 across most leukocyte populations in DNP. Additionally, pp65 NFκB expression was significantly reduced in $CD123^+$ pDCs ($q = 0.0345$, $P = 0.0099$; Fig. 7).

Manual gating found further differences. pp65 NFκB expression was significantly decreased in $CD11c^+$ ($q = 0.0573$, $P = 0.0095$) and $CD11c^-$ ($q = 0.0331$, $P = 0.0055$) mature NK cells; classical ($q = 0.0383$, $P = 0.0096$), intermediate ($q = 0.0430$, $P = 0.0108$), and non-classical ($q = 0.0532$, $P = 0.0089$) monocytes; and $CD123^+$ pDCs ($q = 0.0107$, $P = 0.0018$). pMK2 expression was confirmed to increase across most cell populations with additional significant findings in $CD11c^+CD141^+$ mDCs ($q = 0.0708$, $P = 0.0059$) and $CD19^+$ B cells ($q = 0.0696$, $P = 0.0058$), further indicating its upregulation across most leukocyte populations in DNP patients. Together, these results demonstrate an expansion of NK cell and monocyte populations, as well as increases in pMK2 expression across most cell types, in DNP.

The major findings from the present study are summarised in Fig. 8.

4. Discussion

To our knowledge, this study marks the first time that distinct immunophenotypes have been demonstrated in type 1 diabetes patients with and without neuropathic pain using high-dimensional suspension mass cytometry. It was found that $CD4^+$ central memory T cells, classical and non-classical monocytes, and mature NK cells increased in frequency in the peripheral blood of DNP patients. This was associated with the global upregulation of pMK2, variations in pp65 NFκB expression, and increased expression of CD27, CD127, and CD39 on select T cell populations.

4.1. T cells

There was a phenotypic shift toward $CD4^+$ T cells and a selective expansion of the $CD4^+$ central memory subset in DNP patients. This finding mirrors the expansion of central memory T cells found in complex regional pain syndrome (CRPS) patients (Russo et al., 2019). We also found a decrease in the proportion of $CD8^+$ naïve T cells and increased phospho-p65 NFκB expression in $CD8^+$ central and effector memory T cells. T cells infiltrate the sciatic nerve and dorsal root ganglion in the chronic constriction injury model of neuropathic pain in rats and mice (Moalem et al., 2004). T cell infiltration of the dorsal root ganglion has been associated with pain in the STZ mouse model of T1D (Agarwal et al., 2018), and sural nerve biopsies in DNP patients showed high levels of T cell infiltration, though these were overwhelmingly $CD8^+$ (Younger et al., 1996). Given the known differences in recirculation patterns of activated $CD4^+$ and $CD8^+$ T cells (Gebhardt et al., 2011), it is possible that the inflammatory response is driven by an expanded population of $CD4^+$ T cells that continuously travel between the secondary lymphoid

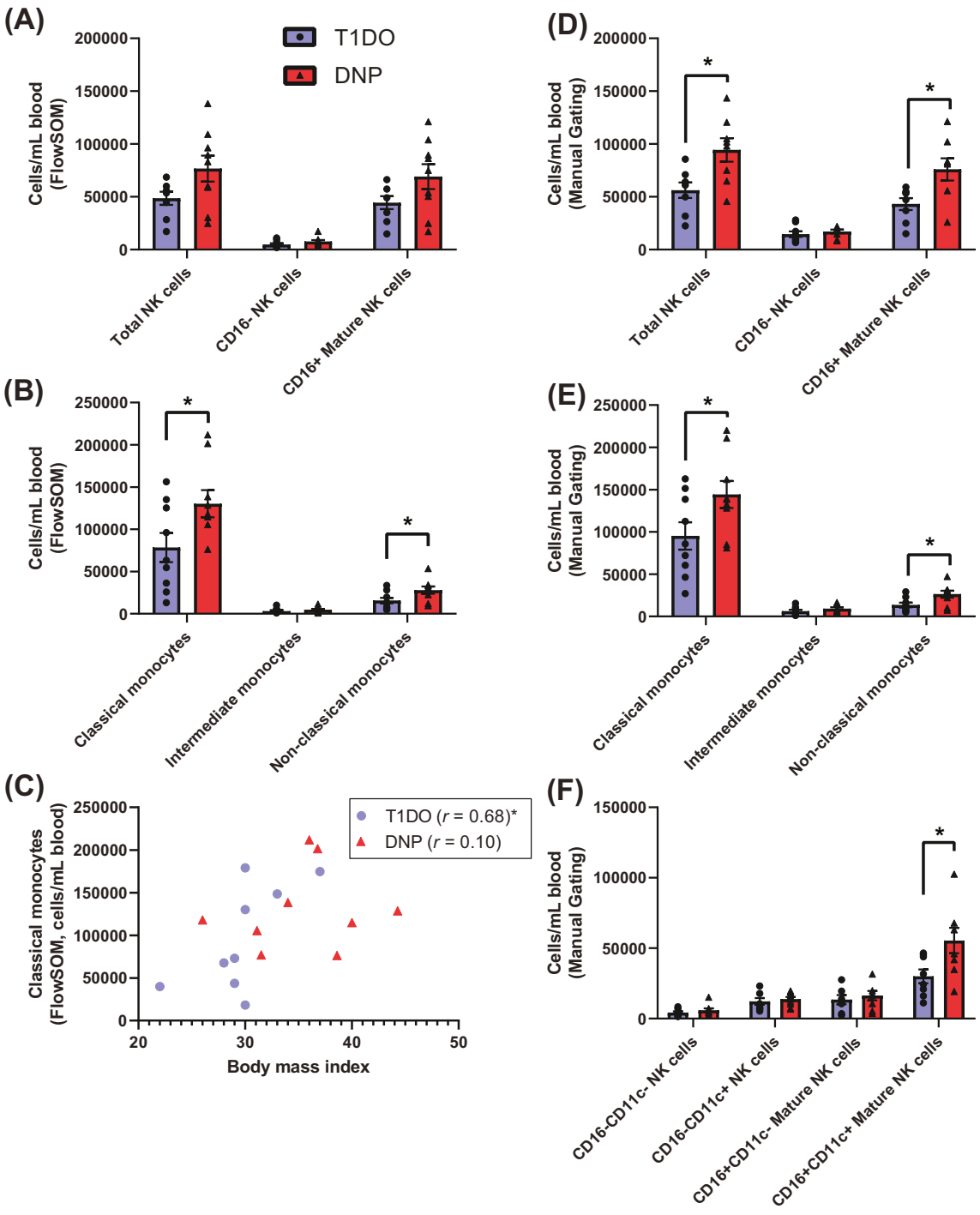

Fig. 6. Cell frequencies for CD19^{-}CD3^{-} natural killer cell and monocyte populations as defined by FlowSOM and manual gating. **(A)** There were no significant differences in the frequency of NK cells, though there was an upward trend in mature NK cells in the DNP group. **(B)** However, significant increases in CD14^{+}CD16^{-} classical and CD14^{-}CD16^{+} non-classical monocyte abundance were revealed. **(C)** There was a significant correlation (Spearman's *r*) between classical monocyte number and BMI in the T1DO control group. This relationship did not hold in the DNP group. **(D)** Manual gating found a significant increase in total NK cell and mature NK cell frequency, **(E)** confirmed the increase in classical and non-classical monocytes, and **(F)** further found that the increase in mature NK cells was the result of a specific significant increase in CD11c^{+} mature NK cells. Values represent group means ± SEM. NK: natural killer; mDC: myeloid dendritic cell; pDC: plasmacytoid dendritic cell. Spearman's *r,* unpaired *t*-test or Mann-Whitney *U* test: *$P < 0.05$.

tissues and inflamed nerves via the blood, instructing CD8^{+} T cells to become activated and enter inflammatory sites where a proportion become resident. Thus, over time, CD8^{+} T cells may become the dominant population in sites of chronic inflammation. Rats with persistent emotional disturbances following nerve injury have higher rates of T cell infiltration than those with no behavioural changes, despite both groups displaying the same level of mechanical allodynia (Austin et al., 2015). The increased levels of depression, anxiety, and stress which were observed in the current DNP cohort may therefore be related to the putative role of T lymphocytes and related cytokine-mediated signalling pathways in influencing coping responses to stressful stimuli such as intractable pain.

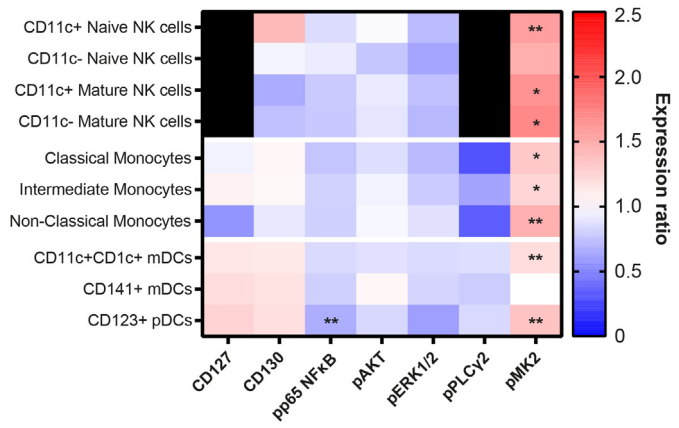

Fig. 7. Heatmap displaying the ratio of group means of arcsinh-transformed median expression values for functional state markers in $CD3^-$ FlowSOM meta-clusters. A ratio of one (white) indicates that the DNP and T1DO group means are the same. A ratio greater than one (red) indicates DNP > T1DO, while a ratio less than one (blue) indicates DNP < T1DO. Black squares denote marker-population combinations with negligible or zero median expression values. Asterisks denote the statistical significance of the difference between group means for a functional state marker in a cell population based on two-way ANOVAs with $q < 0.1$. NK: natural killer; mDC: myeloid dendritic cell; pDC: plasmacytoid dendritic cell. Two-way ANOVA with FDR $q < 0.1$: $^*P < 0.05$; $^{**}P < 0.01$; $^{***}P < 0.001$; $^{****}P < 0.0001$. (For interpretation of the references to colour in this figure legend, the reader is referred to the Web version of this article.)

CD27, a member of TNF-α receptor superfamily whose expression increased on most DNP $CD4^+$ T cells, is an immune checkpoint protein that moderates T cell differentiation, proliferation, and cell survival, and interactions with its ligand increase the activity of NFκB, MAPK, and other proinflammatory signal transduction pathways (Croft, 2009). A combination of anti-neuropathic drugs amitriptyline and nortriptyline decreased $CD4^+CD27^+$ T cells *in vitro*, raising the possibility that CD27 plays some role in neuropathic pain (Royds et al., 2020b). Evidence for CD27 in chronic pain is otherwise limited. It is tempting to speculate that increased CD27 expression on $CD4^+$ T cells increases their receptivity to macrophage-mediated TNF-α generation, thus further contributing to immune dysregulation in DNP.

CD127, the α subunit of the IL-7 receptor, was upregulated specifically on the surface of $CD4^+$ memory T cells. CD127-mediated signalling aids the survival of memory T cells by encouraging proliferative, anti-apoptotic action (Mazzucchelli and Durum, 2007), and selective CD127 blockade on $CD4^+$ memory T cells prevented interferon-γ (IFN-γ) release and reactivity in a chronic inflammatory state without affecting T cell number (Belarif et al., 2018). CD127 increases its expression in the presence of TNF-α in mice (Park et al., 2004), further suggesting a role for TNF-α in these changes.

Additionally, we detected a significant increase in $CD4^+CD127^{hi}CD25^+$ T cells in the DNP group, a population demonstrated to be principally anti-inflammatory and whose frequency is positively correlated with the length of post-T1D diagnosis remission in a young population (Moya et al., 2016; Narsale et al., 2018, 2020). The function of this population in older patients, and its association with macrovascular complications such as DNP in later life, appears worthy of further investigation.

Though we found a decrease in proportion of effector T_{regs} – a very small subset of cells – in the DNP population, no other T_{reg} subsets were significantly different. Previous studies have reported increased numbers of T_{regs} in chronic pain conditions (Luchting et al., 2015; Russo et al., 2019), and in those studies it was suggested that a shift toward anti-inflammatory T cells could be a compensatory mechanism against the stress precipitated by such pain rather than underlying the pathophysiology of chronic pain itself. We were unable to detect differences in type 1 helper T (T_h1) cells, which have a well-documented role in IFN-γ production and known nociceptive effects (Moalem et al., 2004).

4.2. Monocytes

Classical and non-classical peripheral blood monocytes were expanded and dysregulated in DNP patients. Monocytes are effector cells that also act as precursors for myeloid dendritic cells and macrophages, increasing their rate of differentiation during inflammatory activation (Boyette et al., 2017; Teh et al., 2019). In neuropathic pain conditions, there is strong evidence for the involvement of both microglia and blood-derived infiltrating macrophages in the onset of pain (Austin and Moalem-Taylor, 2010; Yu et al., 2020). Monocytes and M1-polarised macrophages are among the major producers of TNF-α in peripheral blood in chronic pain generally (Leung and Cahill, 2010) and specifically in DNP (Shi et al., 2013; Alvarado-Vazquez et al., 2019). Non-classical monocytes have been shown to patrol the endothelial surface of blood vessels and extravasate to release TNF-α and IL-1β in damaged tissues (Teh et al., 2019). Dysregulation of IL-6, IL-10, MCP-1, and TNF-α were observed in peripheral macrophages of type 2 diabetes patients with DNP (Alvarado-Vazquez et al., 2019).

Our laboratory demonstrated an increase in serum levels of granulocyte-macrophage colony stimulating factor (GM-CSF) and IL-8 in a similar cohort of DNP patients (Staats Pires et al., 2020). GM-CSF prompts monocytes to differentiate into macrophages (Boyette et al., 2017; Trus et al., 2020) and acts on macrophages to release pro-inflammatory mediators that can interact with nociceptors (Tewari et al., 2020). A recent study using the STZ mouse model of T1D demonstrated that peripheral monocyte-derived macrophages infiltrate the spinal cord, and that this infiltration is antecedent to mechanical allodynia (Sun et al., 2019). Furthermore, the experimental depletion of these macrophages significantly improved mechanical allodynia, and this was associated with reduced TNF-α and IL-1β expression in the spinal cord (Sun et al., 2019). The depletion of peripheral macrophages with liposome-encapsulated clodronate also delays the development of neuropathic pain in the STZ-induced diabetic rat (Mert et al., 2009). Likewise, in mice fed a high-fat diet, a model of T2DM, macrophage accumulation has been shown to occur in peripheral nerves and to causally contribute to neuropathic pain (Saika et al., 2019). Therefore, the expansion of monocyte populations in the present study warrants further investigation into whether increased differentiation and infiltration of macrophages into human nervous tissues drive local inflammatory processes associated with painful diabetic neuropathy.

Increased monocyte frequency is also observed in T1D patients compared with healthy controls (Min et al., 2012), while hyperglycaemia (Moganti et al., 2017; Grosick et al., 2018) and obesity (Nagareddy et al., 2014; Breznik et al., 2018) are associated with macrophage-mediated inflammation. However, while BMI significantly and positively correlated with monocyte number in T1DO controls in this study, there was no such significant relationship in the DNP group. This suggests that elevated monocyte frequency is not merely the product of an antecedent and more severe obesity-related monocytosis. However, the potential impact of variations in glycaemic control and haemoglobin A1c (HbA1c) levels between groups was not accounted for, so it is possible that these factors have some bearing on the relationship between monocyte frequency and pain.

4.3. Systemic upregulation of MK2

Phosphorylated MK2 was increased across most cell populations in DNP. MK2 is an enzyme downstream of p38 MAPK and its activity is related to post-transcriptional regulation of TNF-α (Ronkina et al., 2007; Menon and Gaestel, 2018). The inhibition of MK2/3 in a mouse model of type 2 diabetes reduced hyperglycaemia and improved insulin functioning (Ozcan et al., 2015). In a mouse model of colon cancer, MK2 was found to have an important role in the regulation of macrophage

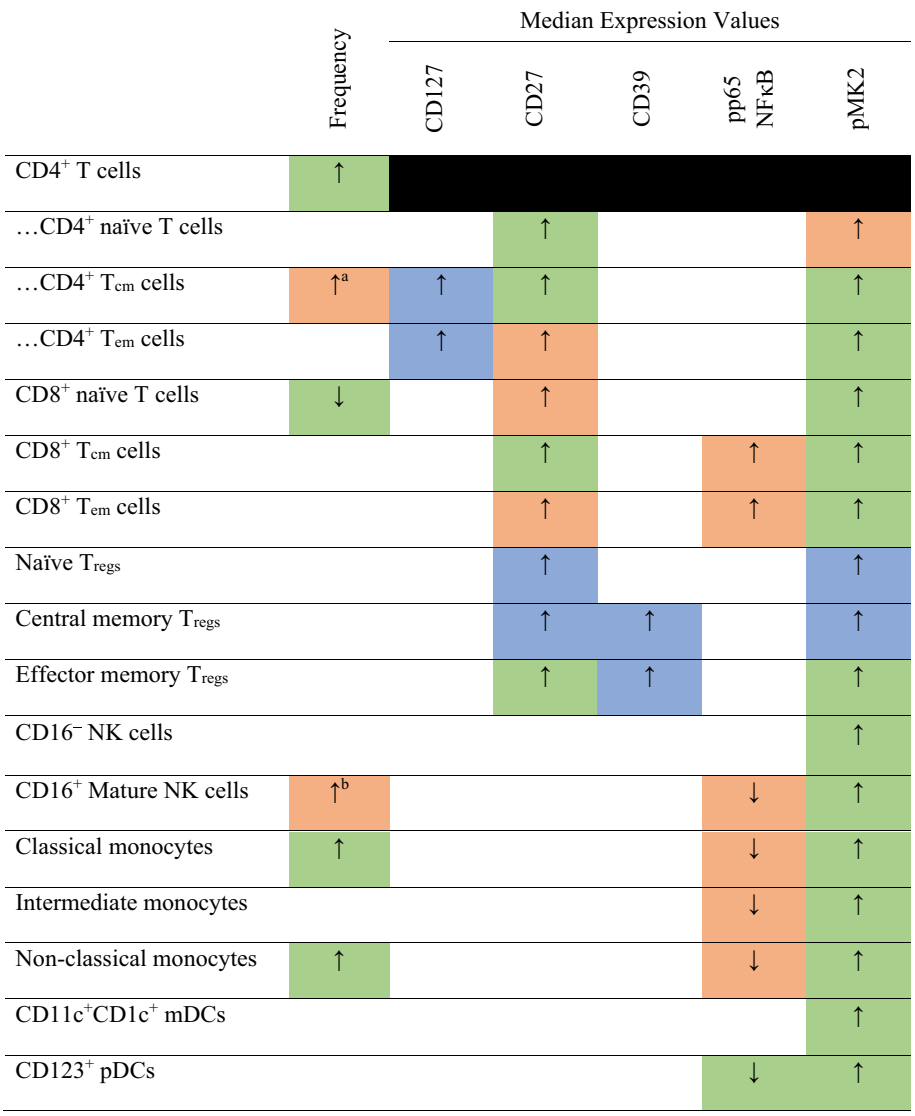

Fig. 8. Summary of major significant results from FlowSOM and manual gating analysis with the level of agreement between analysis methods. Cells are coloured green if group means were significantly different by both FlowSOM and manual gating analysis. Cells are coloured amber if only one of FlowSOM or manual gating showed a significant difference. Cells are coloured blue if they were only investigated by manual gating and showed a significant difference. Parent populations whose frequency was measured, but whose expression data was instead analysed at the subpopulation level, are blacked out. White cells denote no significant difference detected by either classification method. The directionality of SPADE expression aligned with all significant median expression results presented here. ↑/↓: significant increase/decrease in DNP group compared to T1DO controls. T_{cm}: central memory T cells; T_{em}: effector memory T cells; T_{regs}: regulatory T cells; NK: natural killer; mDCs: myeloid dendritic cells; pDCs: plasmacytoid dendritic cells.
[a]FlowSOM significantly different, manual gating $P = 0.0504$. [b]Manual gating significantly different, FlowSOM $P = 0.0931$.

chemotactic protein 1 (MCP-1/CCL2), a chemokine secreted by monocytes and macrophages which recruits antigen presenting cells such as memory T cells, DCs, and other monocytes to sites of injury (Phinney et al., 2018). Mice with spinal cord injury had increased MK2 expression in neurons, astrocytes, microglia, and macrophages around the injury site, and $MK2^{-/-}$ mice with spinal cord injury displayed reduced expression of proinflammatory cytokines around the site of injury and improved locomotor recovery compared to wild type mice (Ghasemlou et al., 2010). Though this evidence all points to a key role for MK2 in similar inflammatory processes in DNP, direct evidence for the involvement of MK2 in DNP, and neuropathic pain in general, remains scant (Lin et al., 2014; Ramesh, 2014). Research to date has instead focused primarily on the role of p38 MAPK in this pathway; for example, the administration of amitriptyline attenuates mechanical allodynia and inhibits the ERK and MAPK pathway in the spared nerve injury rat model of neuropathic pain (Kim et al., 2019), and the use of amitriptyline in human sciatica patients decreased levels of proteins associated with the MAPK pathway in cerebrospinal fluid (Royds et al., 2020a). We were unable to detect phospho-p38 MAPK in the present study due to suboptimal cell staining, so its relationship with MK2 expression in this cohort cannot be determined. Nevertheless, MK2 may be an interesting avenue of future research with respect to DNP and neuropathic pain conditions more generally.

4.4. Additional findings

Mature NK cells, which were elevated in DNP participants, are primed to induce apoptosis in target cells via antibody-dependent cellular cytotoxicity (Davies et al., 2020). Our group previously reported a 50% increase in NK cells in a mass cytometry study of CRPS patients, though the difference between patients and healthy controls was not significant given the high level of variability of this leukocyte compartment between individuals (Russo et al., 2019). There is evidence that the extravasation of NK cells to an injured nerve site may assist in selectively clearing injured axons, thereby decreasing later hyperalgesia (Davies et al., 2019). NK cells appear to coordinate with macrophages in Wallerian degeneration, though what this means for pain outcomes remains unclear; it is possible that specific NK cell phenotypes, yet to be uncovered, drive different outcomes in neuropathic pain states (Davies et al., 2020).

Though we found an increase in phosphorylated p65 NFκB in $CD8^+$ memory T cells, the decrease in mature NK cells, monocytes, and plasmacytoid DCs as defined by manual gating was a surprising finding since evidence for upregulation of NFκB in T1D myeloid cells is well-documented in *ex vivo* and *in vitro* studies. Hyperglycaemia has been associated with an increase in NFκB in T1D patients (Hofmann et al., 1998). Monocytes and immature DCs cultured from T1D patients displayed dysregulated posttranslational activity of NFκB subunits,

including p65, following stimulation with lipopolysaccharide (Mollah et al., 2008). Interestingly, pharmacological inhibition of monocytic NFκB prevented normal differentiation of monocytes to DCs and their subsequent maturation (van de Laar et al., 2010). The decreased monocytic pp65 NFκB in DNP patients in the current study may therefore be related to the observed shift in frequency away from DCs and toward monocytes.

4.5. Study limitations

It is important to note some limitations of this study. The 7-day washout period for anti-inflammatory pharmaceuticals may be insufficient to fully attenuate their effect on some leukocyte populations. Also, neither blood glucose levels nor HbA1c levels – both strong predictors of DNP (Feldman et al., 2019) – were measured. This study therefore cannot comment on the nature of the relationship between glycaemic control and DNP outcomes.

The small sample size (n = 9 per group) made investigating demographic differences untenable. A larger cohort may have revealed sex differences in the mechanisms by which peripheral inflammation is associated with pain in DNP, as is the case in other pain states (Mapplebeck et al., 2016). Participants were geographically and ethnically homogenous, and – despite not being significantly different – were not perfectly aged-matched given that DNP increases prevalence with age. Given these limitations, this study should be considered a preliminary, hypothesis-generating investigation into the immune differences between T1D patients with and without DNP.

5. Conclusions

We present evidence that several leukocyte compartments of the peripheral blood are different between type 1 diabetes patients depending on the presence or absence of painful diabetic neuropathy. $CD4^+$ central memory T cell, monocyte, and mature NK cell populations are expanded and dysregulated in DNP patients, while increases in CD27, CD127, CD39, and pMK2 expression in select populations suggest the involvement of specific inflammatory cascades. These results support the notion that painful diabetic neuropathy has a peripheral immune signature distinct from those that otherwise occur in T1D without pain. Future studies should include a larger, cross-institutional cohort that characterises DNP across wider demographic populations, and/or more specifically directed studies focusing on T cell polarisation, MK2-mediated intracellular pathways including those involving TNF-α, and the potential for peripheral monocytes to differentiate into nerve-infiltrating M1-polarised macrophages in DNP. This would assist in identifying potential neuroimmune mechanisms, and thereby therapeutic targets, to mitigate pain associated with diabetic neuropathy and consequently improve quality of life for affected patients.

Declaration of competing interest

The authors declare no conflicts of interest.

Acknowledgements

We would like to thank all the support staff at Sydney Cytometry and the Ramaciotti Facility for Human Systems Biology for their assistance with the mass cytometry studies.

Appendix A. Supplementary data

Supplementary data to this article can be found online at https://doi.org/10.1016/j.bbih.2021.100283.

Funding

JO'B and PA were supported by the NWG Macintosh Memorial Fund, Discipline of Anatomy and Histology, The University of Sydney, and a Core Facilities Access Scheme grant for Sydney Cytometry from the Core Research Facilities, Research Portfolio, The University of Sydney.

References

Agarwal, N., Helmstadter, J., Rojas, D.R., Bali, K.K., Gangadharan, V., Kuner, R., 2018. Evoked hypoalgesia is accompanied by tonic pain and immune cell infiltration in the dorsal root ganglia at late stages of diabetic neuropathy in mice. Mol. Pain 14, 1744806918817975.

Alvarado-Vazquez, P.A., Grosick, R.L., Moracho-Vilrriales, C., Ward, E., Threatt, T., Romero-Sandoval, E.A., 2019. Cytokine production capabilities of human primary monocyte-derived macrophages from patients with diabetes mellitus type 2 with and without diabetic peripheral neuropathy. J. Pain Res. 12, 69–81.

Amato Nesbit, S., Sharma, R., Waldfogel, J.M., Zhang, A., Bennett, W.L., Yeh, H.C., Chelladurai, Y., Feldman, D., Robinson, K.A., Dy, S.M., 2019. Non-pharmacologic treatments for symptoms of diabetic peripheral neuropathy: a systematic review. Curr. Med. Res. Opin. 35, 15–25.

Antony, M.M., Bieling, P.J., Cox, B.J., Enns, M.W., Swinson, R.P., 1998. Psychometric Properties of the 42-Item and 21-Item Versions of the Depression Anxiety Stress Scales in Clinical Groups and a Community Sample *Psychological Assessment*, vol. 10, pp. 176–181.

Arman, A., Deng, F., Goldys, E.M., Liu, G., Hutchinson, M.R., 2020. In vivo intrathecal IL-1beta quantification in rats: monitoring the molecular signals of neuropathic pain. Brain Behav. Immun. 88, 442–450.

Austin, P.J., Berglund, A.M., Siu, S., Fiore, N.T., Gerke-Duncan, M.B., Ollerenshaw, S.L., Leigh, S.J., Kunjan, P.A., Kang, J.W., Keay, K.A., 2015. Evidence for a distinct neuro-immune signature in rats that develop behavioural disability after nerve injury. J. Neuroinflammation 12, 96.

Austin, P.J., Moalem-Taylor, G., 2010. The neuro-immune balance in neuropathic pain: involvement of inflammatory immune cells, immune-like glial cells and cytokines. J. Neuroimmunol. 229, 26–50.

Barcenilla, H., Akerman, L., Pihl, M., Ludvigsson, J., Casas, R., 2019. Mass cytometry identifies distinct subsets of regulatory T cells and natural killer cells associated with high risk for type 1 diabetes. Front. Immunol. 10, 982.

Belarif, L., Mary, C., Jacquemont, L., Mai, H.L., Danger, R., Hervouet, J., Minault, D., Thepenier, V., Nerriere-Daguin, V., Nguyen, E., Pengam, S., Largy, E., Delobel, A., Martinet, B., Le Bas-Bernardet, S., Brouard, S., Soulillou, J.P., Degauque, N., Blancho, G., Vanhove, B., Poirier, N., 2018. IL-7 receptor blockade blunts antigen-specific memory T cell responses and chronic inflammation in primates. Nat. Commun. 9, 4483.

Bierhaus, A., Humpert, P.M., Morcos, M., Wendt, T., Chavakis, T., Arnold, B., Stern, D.M., Nawroth, P.P., 2005. Understanding RAGE, the receptor for advanced glycation end products. J. Mol. Med. (Berl.) 83, 876–886.

Bouhassira, D., Attal, N., Alchaar, H., Boureau, F., Brochet, B., Bruxelle, J., Cunin, G., Fermanian, J., Ginies, P., Grun-Overdyking, A., Jafari-Schluep, H., Lanteri-Minet, M., Laurent, B., Mick, G., Serrie, A., Valade, D., Vicaut, E., 2005. Comparison of pain syndromes associated with nervous or somatic lesions and development of a new neuropathic pain diagnostic questionnaire (DN4). Pain 114, 29–36.

Boyette, L.B., Macedo, C., Hadi, K., Elinoff, B.D., Walters, J.T., Ramaswami, B., Chalasani, G., Taboas, J.M., Lakkis, F.G., Metes, D.M., 2017. Phenotype, function, and differentiation potential of human monocyte subsets. PloS One 12, e0176460.

Breznik, J.A., Naidoo, A., Foley, K.P., Schulz, C., Lau, T.C., Loukov, D., Sloboda, D.M., Bowdish, D.M.E., Schertzer, J.D., 2018. TNF, but not hyperinsulinemia or hyperglycemia, is a key driver of obesity-induced monocytosis revealing that inflammatory monocytes correlate with insulin in obese male mice. Phys. Rep. 6, e13937.

Croft, M., 2009. The role of TNF superfamily members in T-cell function and diseases. Nat. Rev. Immunol. 9, 271–285.

Crowell, H., Zanotelli, V., Chevrier, S., Robinson, M., 2020. CATALYST: Cytometry dATa anALYSis Tools.

Davies, A.J., Kim, H.W., Gonzalez-Cano, R., Choi, J., Back, S.K., Roh, S.E., Johnson, E., Gabriac, M., Kim, M.S., Lee, J., Lee, J.E., Kim, Y.S., Bae, Y.C., Kim, S.J., Lee, K.M., Na, H.S., Riva, P., Latremoliere, A., Rinaldi, S., Ugolini, S., Costigan, M., Oh, S.B., 2019. Natural killer cells degenerate intact sensory afferents following nerve injury. Cell 176, 716–728 e718.

Davies, A.J., Rinaldi, S., Costigan, M., Oh, S.B., 2020. Cytotoxic immunity in peripheral nerve injury and pain. Front. Neurosci. 14, 142.

Dworkin, R.H., Turk, D.C., Revicki, D.A., Harding, G., Coyne, K.S., Peirce-Sandner, S., Bhagwat, D., Everton, D., Burke, L.B., Cowan, P., Farrar, J.T., Hertz, S., Max, M.B., Rappaport, B.A., Melzack, R., 2009. Development and initial validation of an expanded and revised version of the Short-form McGill Pain Questionnaire (SF-MPQ-2). Pain 144, 35–42.

Feldman, E.L., Callaghan, B.C., Pop-Busui, R., Zochodne, D.W., Wright, D.E., Bennett, D.L., Bril, V., Russell, J.W., Viswanathan, V., 2019. Diabetic neuropathy. Nat Rev Dis Primers 5, 41.

Finck, R., Simonds, E.F., Jager, A., Krishnaswamy, S., Sachs, K., Fantl, W., Pe'er, D., Nolan, G.P., Bendall, S.C., 2013. Normalization of mass cytometry data with bead standards. Cytometry 83, 483–494.

Finnerup, N.B., Attal, N., Haroutounian, S., McNicol, E., Baron, R., Dworkin, R.H., Gilron, I., Haanpaa, M., Hansson, P., Jensen, T.S., Kamerman, P.R., Lund, K., Moore, A., Raja, S.N., Rice, A.S., Rowbotham, M., Sena, E., Siddall, P., Smith, B.H., Wallace, M., 2015. Pharmacotherapy for neuropathic pain in adults: a systematic review and meta-analysis. Lancet Neurol. 14, 162–173.

Fowler, M.J., 2008. Microvascular and macrovascular complications of diabetes. Clin. Diabetes 26, 77.

Ge, S., Xie, J., Zheng, L., Yang, L., Zhu, H., Cheng, X., Shen, F., 2016. Associations of serum anti-ganglioside antibodies and inflammatory markers in diabetic peripheral neuropathy. Diabetes Res. Clin. Pract. 115, 68–75.

Gebhardt, T., Whitney, P.G., Zaid, A., Mackay, L.K., Brooks, A.G., Heath, W.R., Carbone, F.R., Mueller, S.N., 2011. Different patterns of peripheral migration by memory CD4+ and CD8+ T cells. Nature 477, 216–219.

Ghasemlou, N., Lopez-Vales, R., Lachance, C., Thuraisingam, T., Gaestel, M., Radzioch, D., David, S., 2010. Mitogen-activated protein kinase-activated protein kinase 2 (MK2) contributes to secondary damage after spinal cord injury. J. Neurosci. 30, 13750–13759.

Greenbaum, C., Lord, S., VanBuecken, D., 2017. Emerging concepts on disease-modifying therapies in type 1 diabetes. Curr. Diabetes Rep. 17, 119.

Grosick, R., Alvarado-Vazquez, P.A., Messersmith, A.R., Romero-Sandoval, E.A., 2018. High glucose induces a priming effect in macrophages and exacerbates the production of pro-inflammatory cytokines after a challenge. J. Pain Res. 11, 1769–1778.

Hofmann, M.A., Schiekofer, S., Kanitz, M., Klevesath, M.S., Joswig, M., Lee, V., Morcos, M., Tritschler, H., Ziegler, R., Wahl, P., Bierhaus, A., Nawroth, P.P., 1998. Insufficient glycemic control increases nuclear factor-kappa B binding activity in peripheral blood mononuclear cells isolated from patients with type 1 diabetes. Diabetes Care 21, 1310–1316.

Hussain, G., Rizvi, S.A., Singhal, S., Zubair, M., Ahmad, J., 2013. Serum levels of TNF-alpha in peripheral neuropathy patients and its correlation with nerve conduction velocity in type 2 diabetes mellitus. Diabetes Metab Syndr 7, 238–242.

Hussain, G., Rizvi, S.A., Singhal, S., Zubair, M., Ahmad, J., 2016. Serum levels of TGF-beta1 in patients of diabetic peripheral neuropathy and its correlation with nerve conduction velocity in type 2 diabetes mellitus. Diabetes Metab Syndr 10, S135–S139.

Iqbal, Z., Azmi, S., Yadav, R., Ferdousi, M., Kumar, M., Cuthbertson, D.J., Lim, J., Malik, R.A., Alam, U., 2018. Diabetic peripheral neuropathy: epidemiology, diagnosis, and pharmacotherapy. Clin. Therapeut. 40, 828–849.

Janahi, N.M., Santos, D., Blyth, C., Bakhiet, M., Ellis, M., 2015. Diabetic peripheral neuropathy, is it an autoimmune disease? Immunol. Lett. 168, 73–79.

Javed, S., Alam, U., Malik, R.A., 2015. Burning through the pain: treatments for diabetic neuropathy. Diabetes Obes. Metabol. 17, 1115–1125.

Kim, Y., Kwon, S.Y., Jung, H.S., Park, Y.J., Kim, Y.S., In, J.H., Choi, J.W., Kim, J.A., Joo, J.D., 2019. Amitriptyline inhibits the MAPK/ERK and CREB pathways and proinflammatory cytokines through A3AR activation in rat neuropathic pain models. Korean J Anesthesiol 72, 60–67.

Lehuen, A., Diana, J., Zaccone, P., Cooke, A., 2010. Immune cell crosstalk in type 1 diabetes. Nat. Rev. Immunol. 10, 501–513.

Leung, L., Cahill, C.M., 2010. TNF-alpha and neuropathic pain–a review. J. Neuroinflammation 7, 27.

Lin, X., Wang, M., Zhang, J., Xu, R., 2014. p38 MAPK: a potential target of chronic pain. Curr. Med. Chem. 21, 4405–4418.

Luchting, B., Rachinger-Adam, B., Heyn, J., Hinske, L.C., Kreth, S., Azad, S.C., 2015. Anti-inflammatory T-cell shift in neuropathic pain. J. Neuroinflammation 12, 12.

Mapplebeck, J.C., Beggs, S., Salter, M.W., 2016. Sex differences in pain: a tale of two immune cells. Pain 157 (Suppl. 1), S2–S6.

Marca, V., Gianchecchi, E., Fierabracci, A., 2018. Type 1 diabetes and its multi-factorial pathogenesis: the putative role of NK cells. Int. J. Mol. Sci. 19.

Mazzucchelli, R., Durum, S.K., 2007. Interleukin-7 receptor expression: intelligent design. Nat. Rev. Immunol. 7, 144–154.

Menon, M.B., Gaestel, M., 2018. MK2-TNF-Signaling comes full circle. Trends Biochem. Sci. 43, 170–179.

Mert, T., Gunay, I., Ocal, I., Guzel, A.I., Inal, T.C., Sencar, L., Polat, S., 2009. Macrophage depletion delays progression of neuropathic pain in diabetic animals. Naunyn-Schmiedeberg's Arch. Pharmacol. 379, 445–452.

Min, D., Brooks, B., Wong, J., Salomon, R., Bao, W., Harrisberg, B., Twigg, S.M., Yue, D.K., McLennan, S.V., 2012. Alterations in monocyte CD16 in association with diabetes complications. Mediat. Inflamm. 649083. **2012**.

Moalem, G., Xu, K., Yu, L., 2004. T lymphocytes play a role in neuropathic pain following peripheral nerve injury in rats. Neuroscience 129, 767–777.

Moganti, K., Li, F., Schmuttermaier, C., Riemann, S., Kluter, H., Gratchev, A., Harmsen, M.C., Kzhyshkowska, J., 2017. Hyperglycemia induces mixed M1/M2 cytokine profile in primary human monocyte-derived macrophages. Immunobiology 222, 952–959.

Mollah, Z.U., Pai, S., Moore, C., O'Sullivan, B.J., Harrison, M.J., Peng, J., Phillips, K., Prins, J.B., Cardinal, J., Thomas, R., 2008. Abnormal NF-kappa B function characterizes human type 1 diabetes dendritic cells and monocytes. J. Immunol. 180, 3166–3175.

Moya, R., Robertson, H.K., Payne, D., Narsale, A., Koziol, J., Type 1 Diabetes TrialNet Study, G., Davies, J.D., 2016. A pilot study showing associations between frequency of CD4(+) memory cell subsets at diagnosis and duration of partial remission in type 1 diabetes. Clin. Immunol. 166–167, 72–80.

Nagareddy, P.R., Kraakman, M., Masters, S.L., Stirzaker, R.A., Gorman, D.J., Grant, R.W., Dragoljevic, D., Hong, E.S., Abdel-Latif, A., Smyth, S.S., Choi, S.H., Korner, J., Bornfeldt, K.E., Fisher, E.A., Dixit, V.D., Tall, A.R., Goldberg, I.J., Murphy, A.J., 2014. Adipose tissue macrophages promote myelopoiesis and monocytosis in obesity. Cell Metabol. 19, 821–835.

Narsale, A., Lam, B., Moya, R., Lu, T., Mandelli, A., Gotuzzo, I., Pessina, B., Giamporcaro, G.M., Geoffrey, R., Buchanan, K., Harris, M., Bergot, A.S., Thomas, R., Hessner, M.J., Battaglia, M., Serti, E., Davies, J.D., 2020. CD4+CD25+CD127hi cell frequency predicts disease progression in type 1 diabetes. JCI Insight 6 (2), e136114.

Narsale, A., Moya, R., Davies, J.D., 2018. Human CD4(+) CD25(+) CD127(hi) cells and the Th1/Th2 phenotype. Clin. Immunol. 188, 103–112.

Nel, I., Lehuen, A., 2016. Defective invariant natural killer T-cell suppression in patients with type 1 diabetes. Diabetes 65, 2121–2123.

Nicholas, M.K., 2007. The pain self-efficacy questionnaire: taking pain into account. Eur. J. Pain 11, 153–163.

Nowicka, M., Krieg, C., Crowell, H.L., Weber, L.M., Hartmann, F.J., Guglietta, S., Becher, B., Levesque, M.P., Robinson, M.D., 2017. CyTOF workflow: differential discovery in high-throughput high-dimensional cytometry datasets. F1000Res 6, 748.

Olsen, L.R., Leipold, M.D., Pedersen, C.B., Maecker, H.T., 2019. The anatomy of single cell mass cytometry data. Cytometry 95, 156–172.

Ozcan, L., Xu, X., Deng, S.X., Ghorpade, D.S., Thomas, T., Cremers, S., Hubbard, B., Serrano-Wu, M.H., Gaestel, M., Landry, D.W., Tabas, I., 2015. Treatment of obese insulin-resistant mice with an allosteric MAPKAPK2/3 inhibitor lowers blood glucose and improves insulin sensitivity. Diabetes 64, 3396–3405.

Park, J.H., Yu, Q., Erman, B., Appelbaum, J.S., Montoya-Durango, D., Grimes, H.L., Singer, A., 2004. Suppression of IL7Ralpha transcription by IL-7 and other prosurvival cytokines: a novel mechanism for maximizing IL-7-dependent T cell survival. Immunity 21, 289–302.

Phinney, B.B., Ray, A.L., Peretti, A.S., Jerman, S.J., Grim, C., Pinchuk, I.V., Beswick, E.J., 2018. MK2 regulates macrophage chemokine activity and recruitment to promote colon tumor growth. Front. Immunol. 9, 1857.

Qiu, P., 2017. Toward deterministic and semiautomated SPADE analysis. Cytometry 91, 281–289.

Qiu, P., Simonds, E.F., Bendall, S.C., Gibbs Jr., K.D., Bruggner, R.V., Linderman, M.D., Sachs, K., Nolan, G.P., Plevritis, S.K., 2011. Extracting a cellular hierarchy from high-dimensional cytometry data with SPADE. Nat. Biotechnol. 29, 886–891.

Rahman, A.H., Tordesillas, L., Berin, M.C., 2016. Heparin reduces nonspecific eosinophil staining artifacts in mass cytometry experiments. Cytometry 89, 601–607.

Ramesh, G., 2014. Novel therapeutic targets in neuroinflammation and neuropathic pain. Inflamm Cell Signal 1.

Rodacki, M., Svoren, B., Butty, V., Besse, W., Laffel, L., Benoist, C., Mathis, D., 2007. Altered natural killer cells in type 1 diabetic patients. Diabetes 56, 177–185.

Roelofs, J., van Breukelen, G., Sluiter, J., Frings-Dresen, M.H., Goossens, M., Thibault, P., Boersma, K., Vlaeyen, J.W., 2011. Norming of the Tampa Scale for Kinesiophobia across pain diagnoses and various countries. Pain 152, 1090–1095.

Ronkina, N., Kotlyarov, A., Dittrich-Breiholz, O., Kracht, M., Hitti, E., Milarski, K., Askew, R., Marusic, S., Lin, L.L., Gaestel, M., Telliez, J.B., 2007. The mitogen-activated protein kinase (MAPK)-activated protein kinases MK2 and MK3 cooperate in stimulation of tumor necrosis factor biosynthesis and stabilization of p38 MAPK. Mol. Cell Biol. 27, 170–181.

Royds, J., Cassidy, H., Conroy, M.J., Dunne, M.R., Lysaght, J., McCrory, C., 2020a. Examination and characterisation of the effect of amitriptyline therapy for chronic neuropathic pain on neuropeptide and proteomic constituents of human cerebrospinal fluid. Brain, Behavior, & Immunity - Health 100184.

Royds, J., Conroy, M.J., Dunne, M.R., McCrory, C., Lysaght, J., 2020b. An investigation into the modulation of T cell phenotypes by amitriptyline and nortriptyline. Eur. Neuropsychopharmacol 31, 131–144.

Russo, M.A., Fiore, N.T., van Vreden, C., Bailey, D., Santarelli, D.M., McGuire, H.M., Fazekas de St Groth, B., Austin, P.J., 2019. Expansion and activation of distinct central memory T lymphocyte subsets in complex regional pain syndrome. J. Neuroinflammation 16, 63.

Saika, F., Kiguchi, N., Matsuzaki, S., Kobayashi, D., Kishioka, S., 2019. Inflammatory macrophages in the sciatic nerves facilitate neuropathic pain associated with type 2 diabetes mellitus. J. Pharmacol. Exp. Therapeut. 368, 535–544.

Sandireddy, R., Yerra, V.G., Areti, A., Komirishetty, P., Kumar, A., 2014. Neuroinflammation and oxidative stress in diabetic neuropathy: futuristic strategies based on these targets. Internet J. Endocrinol. 674987. **2014**.

Shi, X., Chen, Y., Nadeem, L., Xu, G., 2013. Beneficial effect of TNF-alpha inhibition on diabetic peripheral neuropathy. J. Neuroinflammation 10, 69.

Sia, C., Hanninen, A., 2010. Functional alterations of proinflammatory monocytes by T regulatory cells: implications for the prevention and reversal of type 1 diabetes. Rev. Diabet. Stud. 7, 6–14.

Sommer, C., Kress, M., 2004. Recent findings on how proinflammatory cytokines cause pain: peripheral mechanisms in inflammatory and neuropathic hyperalgesia. Neurosci. Lett. 361, 184–187.

Staats Pires, A., Heng, B., Tan, V.X., Latini, A., Russo, M.A., Santarelli, D.M., Bailey, D., Wynne, K., O'Brien, J.A., Guillemin, G.J., Austin, P.J., 2020. Kynurenine, tetrahydrobiopterin, and cytokine inflammatory biomarkers in individuals affected by diabetic neuropathic pain. Front. Neurosci. 14.

Sullivan, M.J.L., Bishop, S.R., Pivik, J., 1995. The pain catastrophizing scale: development and validation. Psychol. Assess. 7, 524–532.

Sun, J.J., Tang, L., Zhao, X.P., Xu, J.M., Xiao, Y., Li, H., 2019. Infiltration of blood-derived macrophages contributes to the development of diabetic neuropathy. J Immunol Res 7597382. **2019**.

Teh, Y.C., Ding, J.L., Ng, L.G., Chong, S.Z., 2019. Capturing the fantastic voyage of monocytes through time and space. Front. Immunol. 10, 834.

Tesfaye, S., Boulton, A.J., Dickenson, A.H., 2013. Mechanisms and management of diabetic painful distal symmetrical polyneuropathy. Diabetes Care 36, 2456–2465.

Tewari, D., Cook, A.D., Lee, M.C., Christensen, A.D., Croxford, A., Becher, B., Poole, D., Rajasekhar, P., Bunnett, N., Smith, J.E., Hamilton, J.A., McMahon, S.B., 2020. Granulocyte-macrophage colony stimulating factor As an indirect mediator of nociceptor activation and pain. J. Neurosci. 40, 2189–2199.

Trus, E., Basta, S., Gee, K., 2020. Who's in charge here? Macrophage colony stimulating factor and granulocyte macrophage colony stimulating factor: competing factors in macrophage polarization. Cytokine 127, 154939.

van de Laar, L., van den Bosch, A., van der Kooij, S.W., Janssen, H.L., Coffer, P.J., van Kooten, C., Woltman, A.M., 2010. A nonredundant role for canonical NF-kappaB in human myeloid dendritic cell development and function. J. Immunol. 185, 7252–7261.

Van Gassen, S., Callebaut, B., Van Helden, M.J., Lambrecht, B.N., Demeester, P., Dhaene, T., Saeys, Y., 2015. FlowSOM: using self-organizing maps for visualization and interpretation of cytometry data. Cytometry 87a, 636–645.

Waldfogel, J.M., Nesbit, S.A., Dy, S.M., Sharma, R., Zhang, A., Wilson, L.M., Bennett, W.L., Yeh, H.C., Chelladurai, Y., Feldman, D., Robinson, K.A., 2017. Pharmacotherapy for diabetic peripheral neuropathy pain and quality of life: a systematic review. Neurology 88, 1958–1967.

Wiedeman, A.E., Muir, V.S., Rosasco, M.G., DeBerg, H.A., Presnell, S., Haas, B., Dufort, M.J., Speake, C., Greenbaum, C.J., Serti, E., Nepom, G.T., Blahnik, G., Kus, A.M., James, E.A., Linsley, P.S., Long, S.A., 2020. Autoreactive CD8+ T cell exhaustion distinguishes subjects with slow type 1 diabetes progression. J. Clin. Invest. 130, 480–490.

Wong, F.S., Wen, L., 2012. Type 1 diabetes therapy beyond T cell targeting: monocytes, B cells, and innate lymphocytes. Rev. Diabet. Stud. 9, 289–304.

Yamakawa, I., Kojima, H., Terashima, T., Katagi, M., Oi, J., Urabe, H., Sanada, M., Kawai, H., Chan, L., Yasuda, H., Maegawa, H., Kimura, H., 2011. Inactivation of TNF-alpha ameliorates diabetic neuropathy in mice. Am. J. Physiol. Endocrinol. Metab. 301, E844–E852.

Yang, C., Gao, J., Wu, B., Yan, N., Li, H., Ren, Y., Kan, Y., Liang, J., Jiao, Y., Yu, Y., 2017. Minocycline attenuates the development of diabetic neuropathy by inhibiting spinal cord Notch signaling in rat. Biomed. Pharmacother. 94, 380–385.

Young, M.J., Boulton, A.J., MacLeod, A.F., Williams, D.R., Sonksen, P.H., 1993. A multicentre study of the prevalence of diabetic peripheral neuropathy in the United Kingdom hospital clinic population. Diabetologia 36, 150–154.

Younger, D.S., Rosoklija, G., Hays, A.P., Trojaborg, W., Latov, N., 1996. Diabetic peripheral neuropathy: a clinicopathologic and immunohistochemical analysis of sural nerve biopsies. Muscle Nerve 19, 722–727.

Yu, X., Liu, H., Hamel, K.A., Morvan, M.G., Yu, S., Leff, J., Guan, Z., Braz, J.M., Basbaum, A.I., 2020. Dorsal root ganglion macrophages contribute to both the initiation and persistence of neuropathic pain. Nat. Commun. 11, 264.

Zhou, J., Zhou, S., 2014. Inflammation: therapeutic targets for diabetic neuropathy. Mol. Neurobiol. 49, 536–546.

Zhu, T., Meng, Q., Ji, J., Lou, X., Zhang, L., 2015. Toll-like receptor 4 and tumor necrosis factor-alpha as diagnostic biomarkers for diabetic peripheral neuropathy. Neurosci. Lett. 585, 28–32.

Zunder, E.R., Finck, R., Behbehani, G.K., Amir el, A.D., Krishnaswamy, S., Gonzalez, V.D., Lorang, C.G., Bjornson, Z., Spitzer, M.H., Bodenmiller, B., Fantl, W.J., Pe'er, D., Nolan, G.P., 2015. Palladium-based mass tag cell barcoding with a doublet-filtering scheme and single-cell deconvolution algorithm. Nat. Protoc. 10, 316–333.

Zychowska, M., Rojewska, E., Kreiner, G., Nalepa, I., Przewlocka, B., Mika, J., 2013. Minocycline influences the anti-inflammatory interleukins and enhances the effectiveness of morphine under mice diabetic neuropathy. J. Neuroimmunol. 262, 35–45.